Other ACIF Publications in this Series

Stochastic Processes Applied to Physics and Other Related Fields, edited by B. Gómez, S. M. Moore, A. M. Rodriguez Vargas, and A. Rueda (1983).

Workshop on the Search for Gravitational Waves, edited by E. Posada and G. Violini (1983).

Non Conventional Energy Sources, edited by G. Furlan, H. Rodríguez, and G. Violini (1984).

Galaxies, Quasars and Cosmology, edited by L. Z. Fang and R. Ruffini (1985).

Reactor Physics for Developing Countries and Nuclear Spectroscopy Research, edited by K. Lieb and G. Medrano (1986).

Proceedings of the First Latin American School on Biophysics, edited by R. Fayad, A. M. Rodríguez-Vargas, and G. Violini (1987).

METHODS AND APPLICATIONS OF NONLINEAR DYNAMICS

ACIF Series – Volume 7

Medellín, Colombia
September 1-5, 1986

Editor
A. W. SÁENZ
Naval Research Laboratory, Washington, D.C. 20375, U.S.A.
and
Catholic University, Washington, D.C. 20064, U.S.A.

World Scientific
Singapore • New Jersey • Hong Kong

esearch Laboratory for the care with which they typed the relevant editorial changes o create a camera-ready manuscript, and to Mrs. H. S. Oxley of NRL for her valuble help with bibliographical matters.

It goes without saying that it is hoped that this volume will be useful to Latin American scientists and students, as well as those in the United States, Europe, and lsewhere interested in nonlinear physics.

A. W. Sáenz
Naval Research Laboratory
Washington, DC 20375
and
Physics Department
Catholic University
Washington, DC 20064

CONTENTS

ouless, D.J., "Electrons in Disordered Systems and the Theory of
ocalization," Phys. Rep. 13, 93-142 (1974).
ouillard, B, "Electrons in Random and Almost Periodic Potentials", Phys.
ep. 103, 41-46 (1984): "Spectral Properties of Discrete and Random
chrodinger Operators: A Review," preprint for the Proceedings of the
eeting on Random Media of the IMA, Minnesota (1985).
artinelli, F., "A Rigorous Analysis of Anderson Localization," BiBos
52/85.
ouillard, B., "Fractals and Localization," in Amorphous and Liquid
aterials, Proceedings of the NATO ASI, edited by E. Lutscher, G. Fritsch,
nd G. Jacucci (Nijhoff, Dordrecht, Netherlands, 1987, pp. 19-28.
archesoni, F., and Vázquez, L., "Sine-Gordon Solitons in the Pre-
ence of a Noisy Potential," Physica 14D, 273-276 (1985).
ascual, P.J., and Vázquez, L., "Sine-Gordon Solitons under Weak
tochastic Perturbations," Phys. Rev. B32, 8305-8311 (1985).
odríguez, M.J., and Vázquez, L., "Behavior of the φ^4-Kinks Under
tochastic Perturbations," in preparation.
ass, F.G., Konotop, V.V. and Sinitsyn, Yu. A., "Solitons in a Ran-
om Force Field," Sov. Phys. JETP 61, 318-322 (1985).
odd, R.K., Eilbeck, J.C., Gibbon, J.D. and Morris, H.C., Solitons
nd Nonlinear Wave Equations (Academic, London, 1982).
uo Ben-Yu, Pascual, P.J., Rodríguez, M.J., and Vázquez, L., "Nume-
ical Solution of the Sine-Gordon Equation," Appl. Math. Comp. 18,
-14 (1986).
elfand, E., "Numerical Integration of Stochastic Differential Equa
ions," Bell Sys. Tech. J. 58, 2289-2299 (1979).

CHAOS IN SOLID STATE SYSTEMS

A. Zettl
Department of Physics
University of California, Berkeley
Berkeley, Calif. 94720 U.S.A.

An introduction to chaotic dynamics in driven solid state systems is presented. First, methods of chaos identification and analysis are described. The methods are then applied to driven Josephson junctions, charge density waves, and semiconductors. Both temporal and spatial chaos are investigated. The sensitivity of the dynamical response to external noise, far from or near to a dynamical instability, is also discussed.

CONTENTS

INTRODUCTION

The inherent complexity of the "turbulent" dynamical response of uids, flame fronts, or even biological systems has long been preciated. Recent advances in the theory of chaos have generated a w understanding of and appreciation for complex nonlinear dynamics. thods of analysis have been developed which allow direct termination of important system parameters (such as number of active grees of freedom) from the seemingly erratic response. The richness classical dynamics in the chaotic regime has suggested interesting rallels with well established theories of quantum dynamics.

Chaotic dynamics appears to be a very general phenomenon. In this ief review,we shall explore chaotic dynamics in solid state systems. olid state turbulence" is a relatively new field of study and only a ndful of chaotic solid state systems have actually been identified. vertheless, a wealth of experimental data and theoretical results ist. This paper is not meant to be an exhaustive review of that rk, but merely to serve as an introduction to this exciting and pidly growing field.

Three classes of solid state systems form the focus of this paper: sephson junctions, charge density waves, and semiconductors

(including p-n junctions, photoconductors, and electron-hole plasmas). In general the equations of motion for these systems are derived from a quantum framework, but have simple classical analogs. An attempt has been made to keep the "chaos" language as simple as possible and to focus only on the features of the solid state systems directly relevant to the chaotic response.

2. CHAOTIC RESPONSE-- IDENTIFICATION AND ANALYSIS

2.1 A Hypothetical Experiment

Let us consider a "black box" system as shown in Fig. 1. The system may be a complicated one, with many degrees of freedom. The

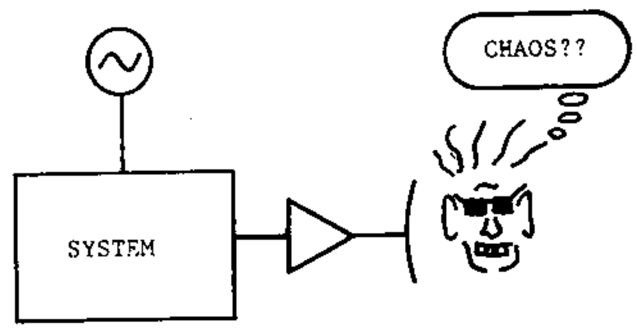

Figure 1. Testing a system for chaos.

exact equations of motion are unknown, but it is assumed that the system is dissipative. The box has one input port and one exit port. The input port is connected to a sine wave oscillator; the exit port is connected to an audio amplifier and Hi-Fi speaker. We listen to the speaker. With the oscillator amplitude knob set to zero, we hear nothing. As the amplitude is steadily increased, we hear first a elatively pure tone corresponding to the oscillator frequency at ω_{ex}, hen also higher harmonics, then also a lower frequency, and then loud, cratchy noise. Have we discovered chaos in the box? How many active legrees of freedom does the system possess? Can we determine this and nore from just the single output variable, the acoustic wave amplitude rersus time? Would it be advantageous to have more than one output port on the box, each corresponding to a different "part" of the system? In this and the following sections, we shall develop concepts and methods which address these questions, and apply them to selected solid state systems.

2.2 Chaotic Dynamics

We here treat a dynamical system with dissipation and potentially many degrees of freedom. The system is self-driven, externally driven, or both. The temporal evolution of the system is represented as a trajectory of a point in multidimensional phase space. Figure 2 shows one such possible trajectory in a three dimensional phase space.

Different initial conditions will correspond to different deterministic trajectories in the phase space. Since the system is dissipative, the volume occupied in phase space by the trajectories will converge to a limit set, i.e. to an attractor.[1] If the system is chaotic, the attractor to which the trajectories converge is a strange attractor.[2] Figure 3 shows a typical strange attractor. The

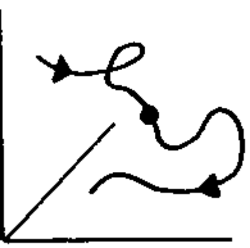

Figure 2. Trajectory of system in phase space.

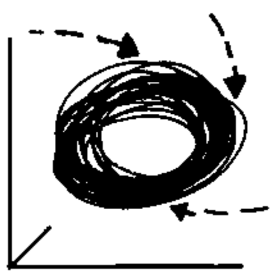

Figure 3. Attractor in phase space.

strange attractor has some interesting properties, which result from the multiple foldings in phase space which the attractor has undergone. If particular, on a strange attractor nearby trajectories simultaneously diverge exponentially from one another, but remain bounded in phase space. the rate of divergence (or convergence) of the trajectories is measured by the Lyapunov exponents.[3] For chaos to exist, there must be at least one positive Lyapunov exponent (i.e., there must be divergence present).

The fact that nearby trajectories on a strange attractor may diverge leads to a sensitive dependence on initial conditions. This means that if, at a given time, all the phase space coordinates are known exactly (possible only in a classical framework), then the evolution of the system is fully determined. However, an infinitesimal uncertainty in even one of the coordinates leads to an exponential growth in the uncertainty of the trajectory. This implies that even if the system returns almost exactly to the same initial condition (near recurrence), the resulting orbit in phase space will not be almost periodic. Rather, the response will sample nearly all orbits, leading to broadband (noisy) response. This gives us our first test for the existence of chaos: a broadband response spectrum.

In the hypothetical experiment of Section 2.1, we could have connected the output of the amplifier to a spectrum analyzer (Fourier transform); the resulting power spectra might be as shown in Fig. 4. In Fig. 4d, broadband noise is observed. Does this mean that the system is chaotic? The answer is probably yes, but more analysis is necessary. Broadband response is a signature, but not proof, of chaos.

Another important feature of a strange attractor is that it has a fractal dimension.[3] In a sense, the attractor has a certain nonintegral "roughness" to it, which can always be recovered by a suitable change of magnification scale. The utility of determining the dimension of a strange attractor (other than insuring that the attractor is indeed strange) is that the dimension gives approximately the number of active degrees of freedom in the system. For example, a

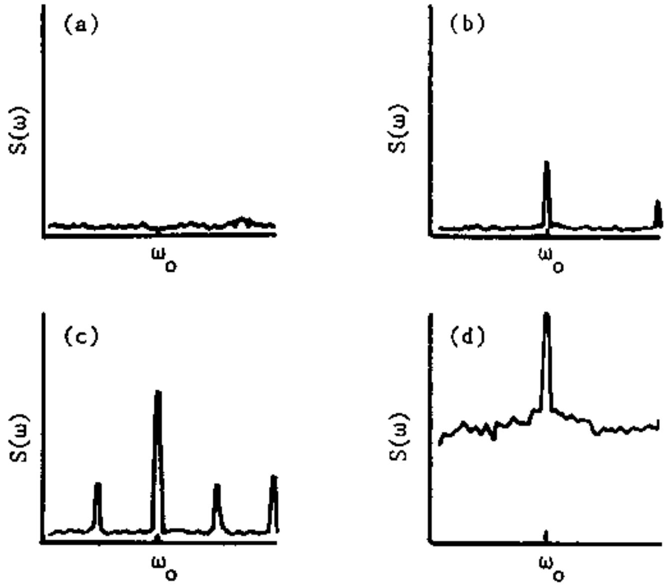

Figure 4. Response power spectra for four different drive amplitudes. a) zero drive; b) drive = 1; c) drive = 2, period doubling; d) drive = 3, chaos.

ulent fluid might be thought to have essentially an infinite number egrees of freedom, but the deterministic chaotic response might be ribed by only a few active degrees of freedom. This is the meaning low dimensional chaos".

How does one experimentally determine the dimension of the actor? The attractor is in general a complicated object residing ultidimensional phase space. A simplification occurs in viewing attractor if it is projected onto a two dimensional space, defined wo independent variables, thus creating a phase portrait.[1-4] The pendent variables might be, for example, the voltage V(t) supplied he drive oscillator and the current response I(t) of the system. possible phase portraits are shown in Fig. 5. In Fig. 5b, the

orbit is periodic. The phase portrait gives a projected view of the attractor. Dimensional information can be obtained from a Poincaré section,[1-4] generated by placing a two-dimensional surface in multi-dimensional phase space and recording on the surface (with a dot, say) each time the trajectory unidirectionally pierces the surface. In practice this can be accomplished by "strobing" the phase portrait, using as the strobe trigger the drive oscillator frequency or a dominant frequency internal to the system. Figure 6 shows Poincaré sections corresponding to the phase portrait of Fig. 5.

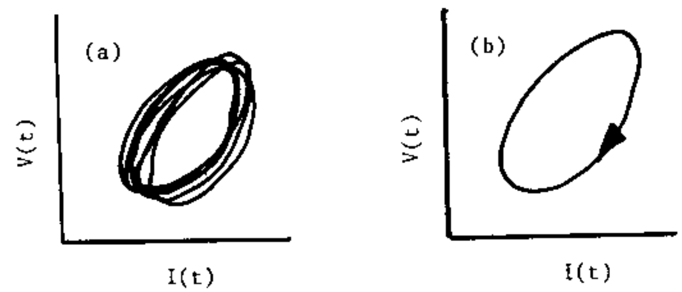

Figure 5. Current response versus voltage drive, yielding phase portrait.

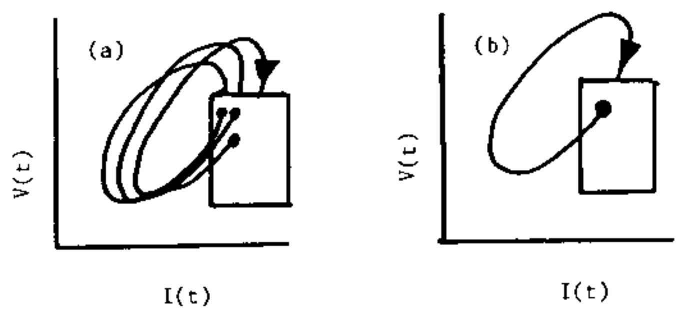

Figure 6. Poincaré section of attractor.

The Poincaré section gives a slice, rather than a projection of e attractor. The <u>return map</u>[1,4] relates the state of the system at dex n+1 (n could be a time unit) to the state of the system at index

The return map of the system described in Fig. 6b, for example, is pecially simple. As shown in Fig. 7a, the return map here consists only one point. Figure 7b shows a more complex return map. Note at the points on this

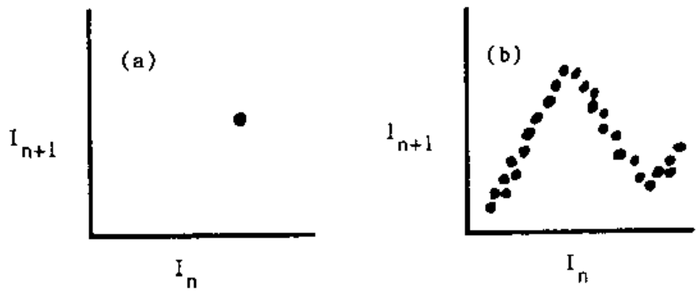

Figure 7. Return map.

pping fall more or less on a continuous line; this is an example of a e-dimensional return map. The return map in general corresponds to ccessive iterates of the system. If the return map for a system is own, its evolution can be tracked "geometrically" using only a raight edge. This is illustrated in Fig. 8. Iterating a map is in neral far easier than integrating the (often highly complex) fferential equations governing the system.

How does one experimentally generate a Poincaré section or return p? To extract the Poincaré section, one needs only to display two dependent variables of the system (say voltage and current) on the rtical and horizontal axes of an oscilloscope, and strobe the cilloscope with an appropriate frequency trigger. The return map

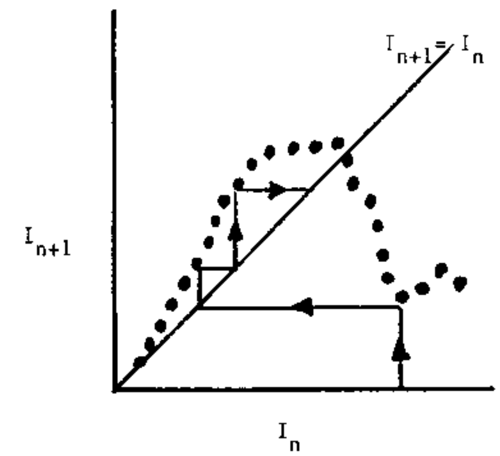

Figure 8. Iterating a map.

can, rather surprisingly, be generated or reconstructed from only a single variable of the system.[5,6] If the output of the system is converted to a voltage $V(t)$, then the time series $V(t_i + T)$, $V(t_i + 2T)$, $V(t_i + 3T)$,..., $V(t_i + (m-1)T)$ defines a return map, provided $m > D$, with D the embedding dimension. This type of reconstruction of phase space is a particularly powerful experimental tool.

The fractal dimension d_F of the attractor can be extracted from the Poincaré section or from the reconstructed phase space (return map). A number of box-counting algorithms have been suggested. Strictly speaking, the fractal dimension can be expressed as[3]

$$d_F = \lim_{\varepsilon \to 0} \frac{\log M(\varepsilon)}{\log (1/\varepsilon)} , \tag{2.1}$$

where the phase space has been divided up into P-dimensional cubes of side ε, where P is the dimension of the phase space in which the attractor lies. $M(\varepsilon)$ is the number of cubes visited by the attractor.

nfortunately, Eq. (2.1) is difficult to apply to an experimental ituation. A useful practical technique is to reconstruct the -dimensional phase space from a single variable, and then calculate he pointwise dimension, or natural measure.[3] One then assumes that he pointwise dimension is a good approximation to d_F. The pointwise imension is determined by randomly selecting a point on the attractor, nd then placing a P-dimensional hypercube (or hypersphere) of radius r round that point. The number of other points N(r) from the attractor ithin that cube is then evaluated. With

$$N(r) \sim r^{d_F} , \qquad (2.2)$$

plot of log N(r) versus log r yields a straight line of slope d_F. An nportant distinction between the pointwise dimension and d_F is that d_F s a global dimension (refers to the entire attractor), whereas the pintwise dimension is a local quantity. Fortunately, many attractors ave a uniform dimension throughout, and thus the the local measure is quivalent to the global measure.

The topological nature of the attractor is dictated by the arameters defining the system. Often, changes in these parameters rastically alter the system and hence also the attractor. We may efine a parameter λ as a control parameter; of interest is how the ystem and its attractor are changed as λ is changed. For example, in ne sequence of Fig. 4, λ might be the oscillator amplitude voltage. f we were to plot the output of the system (say the current response) s a function of time, then the traces of Fig. 9 might result. Note hat local minima in the current response have in Fig. 9 been nderlined. These minima define a bifurcation diagram.[1-4] The ifurcation diagram expresses, for example, the local minima versus the ontrol parameter. An example is given in Fig. 10, where λ_0, λ_1, λ_2, nd λ_3 are identified. At each bifurcation (splitting)point, the ystem period doubles, and the topllogical nature of the attractor is

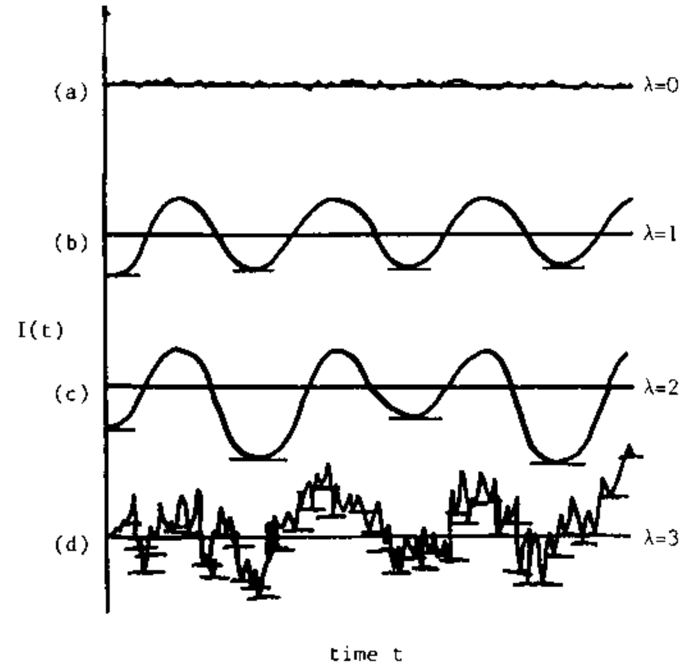

Figure 9. Real-time response for four values of the control parameter λ. Local minima are underlined.

drastically altered. Bifurcation diagrams provide a very useful visual display of the behavior of the system for various control parameters.

3. THE ANHARMONIC OSCILLATOR

Although the assumption of a harmonic potential is often a useful simplification in the description of real physical systems, that

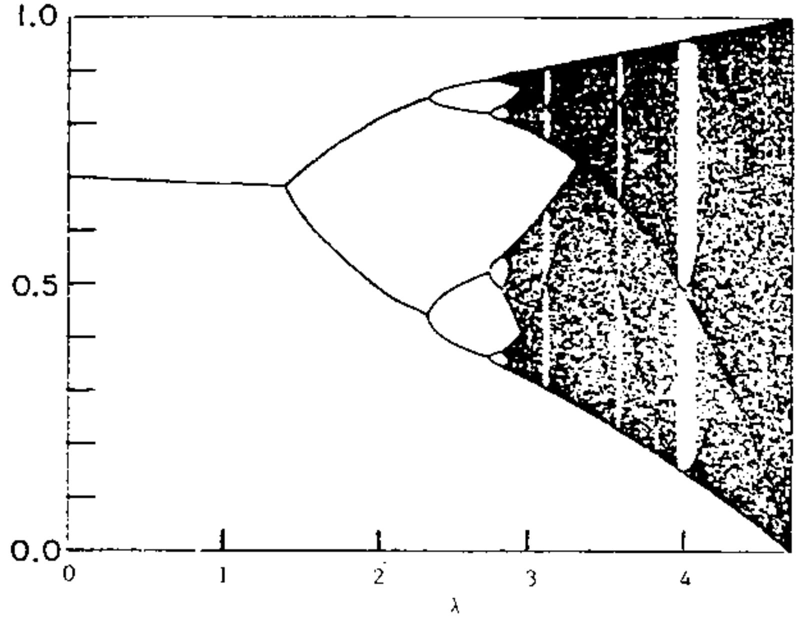

Figure 10. Bifurcation diagram.

plification eliminates chaotic response! The anharmonic potential, the other hand, is often more realistic, and usually leads to a rich ctrum of nonlinear response phenomena, including chaos. Huberman Crutchfield [7] studied the solutions of a driven anharmonic illator nearly a decade ago, and identified the existence of a ange attractor and chaotic solutions.

We consider here the anharmonic restoring potential

$$U = \frac{1}{2}\phi^2 - \frac{1}{4}\phi^4 \tag{3.1}$$

the related periodic potential

$$U = 1 - \cos\phi \,. \tag{3.2}$$

In certain approximations, the potential of Eq. (3.2) applies to two well-known solid state systems, Josephson junctions and charge density waves.

3.1 Josephson Junctions

A Josephson junction is an electronic device fabricated by sandwiching an insulating layer between two superconductors.[8] The resulting junction can be modelled by an ideal junction in parallel with a (quasiparticle) leakage resistance R and a junction capacitance C. The ideal junction obeys $I = I_c \sin\theta$ and $V = h\dot{\theta}/2e$, with I_c the junction current, V the junction voltage, and θ the superconducting phase difference across the junction. I_c is the critical current (beyond which a finite voltage appears across the junction). The resulting "RSJ" (for resistively shunted junction) equation of motion for the real junction becomes

$$\frac{\hbar C}{2e}\ddot{\theta} + \frac{h}{2eR}\ddot{\theta} + I_c \sin\theta = I \,, \tag{3.3}$$

with I the external drive current, $I = I_{dc} + I_{ac}\cos(\omega t)$. In appropriately redefined units (including time), Eq. (3.3) becomes

$$\beta\ddot{\phi} + \dot{\phi} + \sin\phi = I/I_c \,, \tag{3.4}$$

where β is a damping parameter. Equation (3.3) is isomorphic to that which describes a damped physical pendulum. In many cases it is assumed that

3.4) describes so well the real junction that the detailed ior of the junction and numerical integrations of the equation are as equivalent.

quation (3.4) displays extremely complex nonlinear behavior,[9-13] and of these features have recently been observed in real junctions. portant experimental difficulty with real junctions is, however, the characteristic frequency is so high that only limited data sition and analysis is possible.

Figure 11 shows an early analog-computer determination[14] of the nse of Eq. (3.4) for ac drive only, where $I = I_{ac} \cos(\omega t)$. At encies close to the natural oscillation frequency ω_0, an easing ac amplitude leads to chaos. Later work[9-13] has shown the situation is far more complicated than Fig. 11 would suggest, he general result of chaotic solutions for ω close to ω_0 and for ciently high ac drive still holds. Ac-induced chaos probably does in real Josephson junctions, but it has not yet been clearly rved.

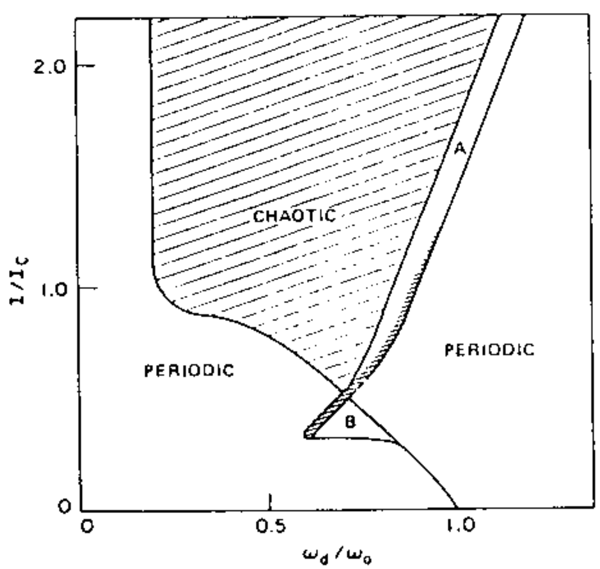

Figure 11. Response of Eq. (3.4) for $\beta^2 = 5$. From Ref. 14.

For combined ac and dc drive, i.e., for $I = I_{dc} + I_{ac} \cos(\omega t)$, Eq. (3.4) again predicts highly complex response. Mode-locked steps result whenever the external frequency matches the internal ac Josephson frequency.[8] Chaotic response can occur on the steps, causing excessive noise, or even leading to a destruction of the stability of the step.[9,13] Figure 12a shows such behavior in a Pb/Te/Pb Josephson junction.[15] Figure 12b shows the corresponding prediction of Eq. (3.4), which is seen to be in good agreement with experiment. Again, because of the very high frequencies involved in Josephson junction experiments (typically GHz), very little of the sophisticated analysis discussed in the previous section appears possible. Of course, a great deal of such analysis has been performed on Eq. (3.4), where the frequency is normalized to a convenient unit in the analog or digital computations.

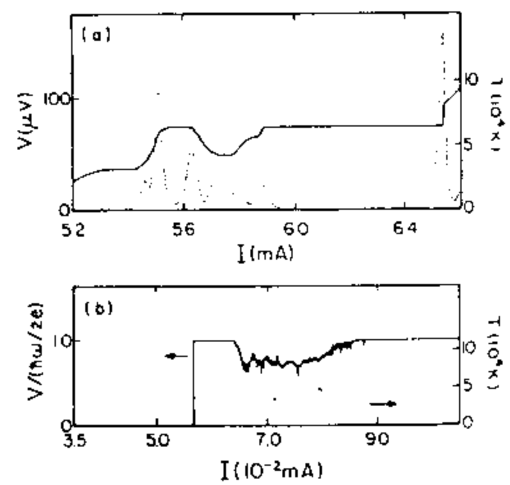

Figure 12. I-V characteristic (solid line) and noise temperature (dotted line) for Josephson junction driven by ac and dc current. (a): real Pb/Te/Pb junction; (b): theory. From Ref. 15.

3.2 Charge Density Waves

A charge density wave (CDW) is a modulation of the electronic charge density which results from a Peierls distortion in a solid state crystal. CDW transitions are a common phenomenon in a variety of low dimensional conductors.[16] The low dimensionality is important because good Fermi surface nesting helps drive the transition. In the quasi-1D conductor $(TaSe_4)_2I$, for example, there occurs a Peierls distortion at $T_P = 265K$; below T_P a collective-mode CDW state exists.

Electrons "condensed" in the CDW state respond to applied elecric fields in a coherent and unusual way. The phase of the CDW may be pinned to the underlying lattice by impurities, and only for dc fields $E_{dc} > E_T$, with E_T the threshold field, will the CDW electrons move and carry a current. Hence the CDW system is highly nonlinear. A moving CDW also generates an intrinsic narrow-band frequency, which is directly proportional to the CDW drift velocity. For low amplitude ac fields, the CDW responds much like an overdamped harmonic oscillator. In the simplest approximation, an equation of motion for the CDW phase may be written as[17]

$$\beta\ddot{\phi} + \dot{\phi} + \sin\phi = E/E_T, \qquad (3.5)$$

where $E = E_{dc} + E_{ac}\cos(\omega t)$. Note that with appropriate redefinition of variables, this equation is identical to Eq. (3.4), which describes the dynamics of Josephson junctions. Equation (3.5) is admittedly a very crude approximation to CDW dynamics in that it fully neglects internal degrees of freedom for the CDW. Nevertheless, it does predict a threshold field E_T, generation of an intrinsic frequency linear in CDW drift velocity, and a harmonic-oscillator-type ac conductivity.

For sufficiently large ac driving fields, the CDW pinning potential is anharmonic, and one might therefore expect chaotic response for an ac driven CDW. In general, however, this is not observed (it has been searched for in $NbSe_3$, $(TaSe_4)_2I$, TaS , and $K_{0.3}MoO_3$, all sliding CDW systems). The problem lies in the excessive damping associated with CDW dynamics. If damping is too large, Eq. (3.5) does <u>not</u> predict chaos. This is illustrated in Fig. 13, which shows[12] the state diagram for Eq. (3.5) in the amplitude-damping plane (low β corresponds to large damping; $\rho \propto E_{ac}$). For large damping, a very large ac amplitude is required for non-periodic response.

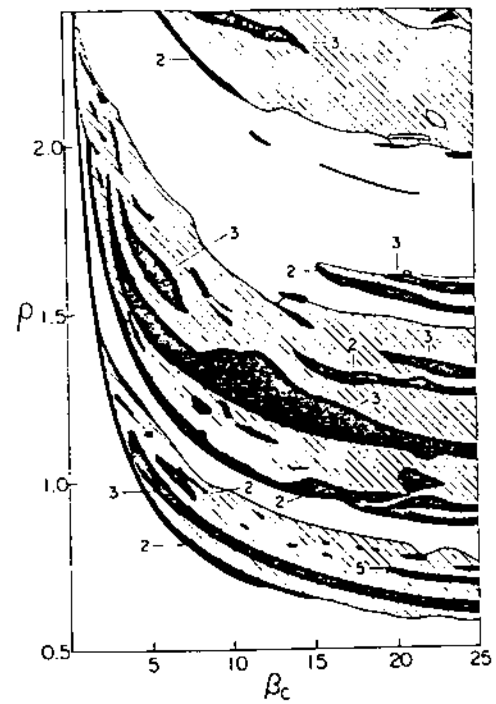

Figure 13. State diagram of Eq. (3.5) in the drive amplitude-damping plane. The hatched regions are chaotic. From Ref. 12.

In $(TaSe_4)_2I$, the overall damping can be modified by placing the CDW crystal in series with an inductance.[18] The inductance simulates CDW inertia. The resulting hybrid circuit does display chaos, as illustrated in Fig. 14. The general form of the response should be compared to Fig. 11, which is the prediction of Eq. (3.5) with small damping.

CDW systems offer distinct advantages over Josephson junctions in the study of chaos, in that the characteristic CDW frequencies are in

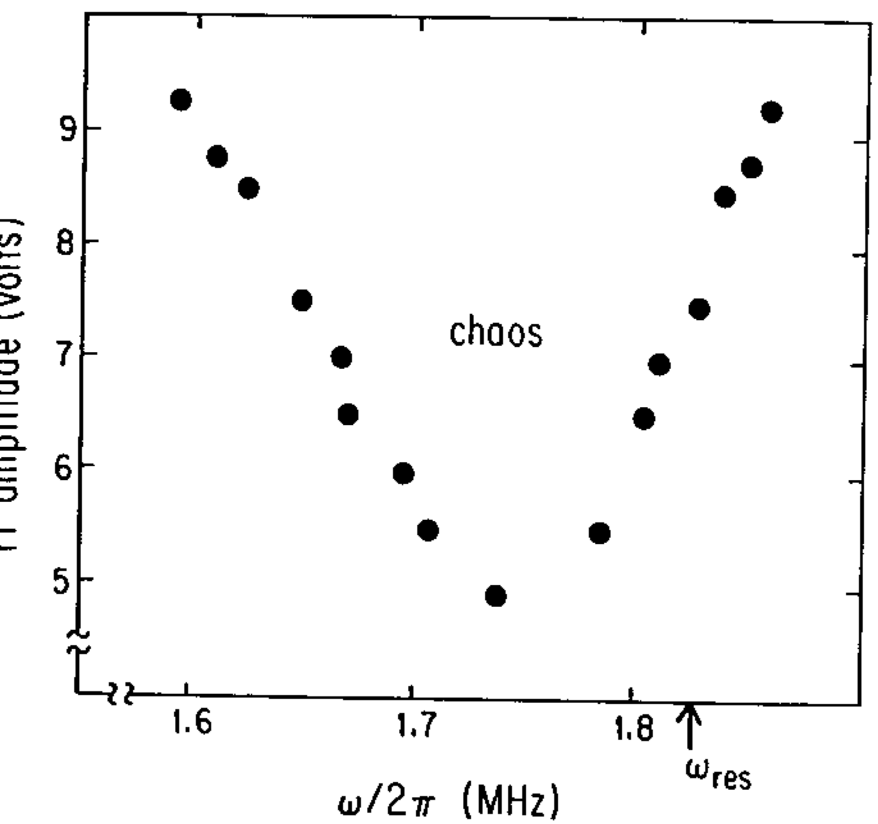

Figure 14. Chaotic-periodic response boundary for a $(TaSe_4)_2I$ circuit. From ref. 18.

the low MHz range. In sharp contrast to the GHz range of Josephson junctions, a host of rf electronics is available for detailed MHz chaos analysis.

4. MODE LOCKING

Mode locking is a rather general phenomenon which can occur in systems with competing periodicities. Let us consider a system with an internal periodicity or frequency ω_{in}, driven externally by a source at frequency ω_{ex}. Depending on the coupling between the external drive and the system, the internal frequency can "lock" to ω_{ex}. This is the process involved in biological pacemakers, where the (otherwise erratic) internal frequency of the heart is locked to the carefully selected drive frequency of an electronic pulse generator.

We shall here discuss mode locking in the language of the circle map, which provides a concise yet far reaching description of chaotic behavior in a variety of real systems.

4.1 Circle Map

Imagine the quasi-periodic behavior of a system with an internal frequency $\omega_{in} \sim \dot{\Theta}_1$ driven by an incommensurate source at frequency $\omega_{ex} \sim \dot{\Theta}_2$. The motion of the system in phase space can be represented as motion of a 2-D torus, as illustrated in Fig. 15. We may select a Poincaré section at the plane $\Theta_2 = 0$, and strobe the system at "times" $\Theta_2 = 0, 2\pi, 4\pi$, etc. As the system evolves, each intersection point on

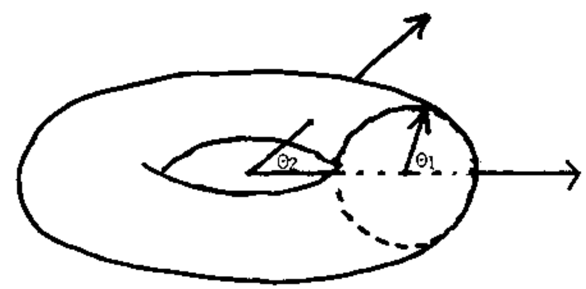

Figure 15. Motion on a 2-D torus. The intersection with the plane $\Theta_2 = 0$ defines the circle (or topological equivalent).

circle (the circle is defined by the intersection of the torus with
plane) is mapped to another point on the same (invariant) circle.
thus have a nonlinear map of the circle onto itself .

One such mapping of the invarient circle is the sine circle
,19)

$$\theta_{n+1} = \theta_n + \Omega + \frac{K}{2\pi} \sin 2\pi\theta_n \,, \qquad (4.1)$$

re θ_n describes the state of the system at index n, $\Omega = \omega_{in}/\omega_{ex}$, and
s the "strength" of the coupling between the system and the external
ve. The sine circle map has been extensively studied, and predicts
nsitions to chaos.[19-22]

Figure 16 shows numerous iterations of the sine circle map with $\Omega =$
and $K = 0.9$.[21] Quasi - periodic behavior is observed. With
reasing K, the map develops a local maximum; hence it is no longer
ertible and may develop chaos. For certain values of K and Ω, the
cle map predicts <u>mode locking</u>, where ω_{in} is related to ω_{ex} by
$/\omega_{ex} = p/q$, with p and q integers. Figure 17 shows some of the mode-
ked regions of the circle map in K-Ω space.[21] The locked regions
often referred to as "Arnold tongues" or "entrainment horns". For
ge K, the tongues or resonances overlap, and this overlap can lead
hysteresis and chaos (hopping between resonances). If all p/q
os had been plotted in Fig. 17, the resonances would start
rlapping at K = 1, the critical line. Only for $K > 1$ is chaos
sible in the sine circle map.

The mode-locked regions at K = 1 in the circle map form a Cantor
23) with a fractal dimension. Figure 18 shows the set of locked
ons; the set forms a "<u>devil's staircase</u>". The dimension of the
plete) staircase at K = 1 has been computed as $d_F = 0.860$.[20-22]

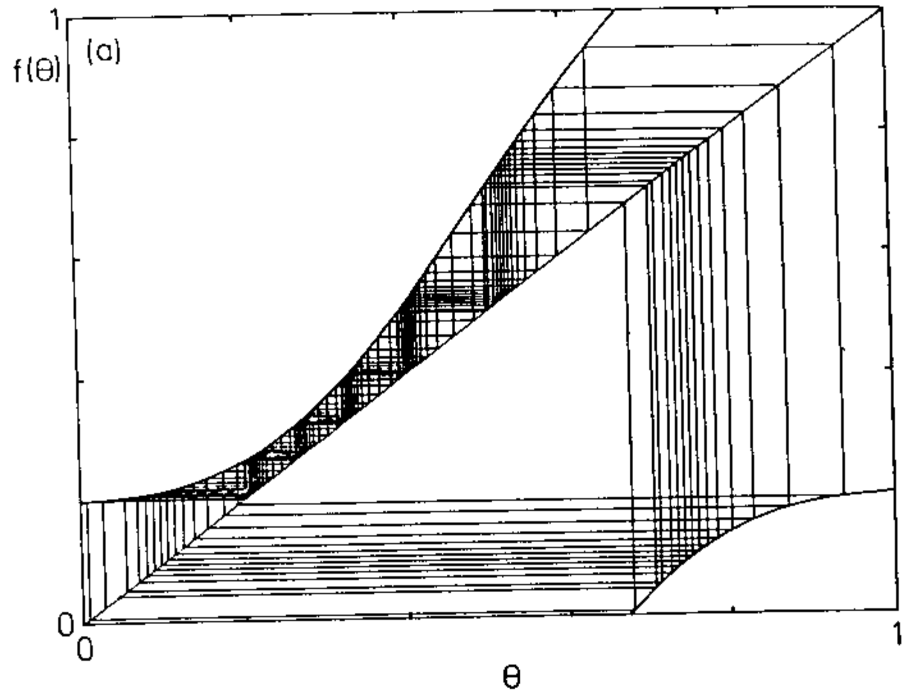

Figure 16. Iterating the sine circle map in the quasi-periodic regime ($K = 0.9$, $\Omega = 0.2$). From Ref. 21.

It has been clearly demonstrated that the sine circle map does apply to a number of real physical systems, in particular fluid instabilities [24] and some semiconductors.[25] We now consider its potential applicability to Josephson junctions and charge density waves.

4.2 Josephson Junctions and Charge Density Waves

Mode locking phenomena occur in Josephson junctions and are well known in the Josephson literature.[8] In general the experiment is performed by irradiating the junction with microwaves at frequency ω_{ex}, and measuring the dc I-V characteristics. The locked regions are

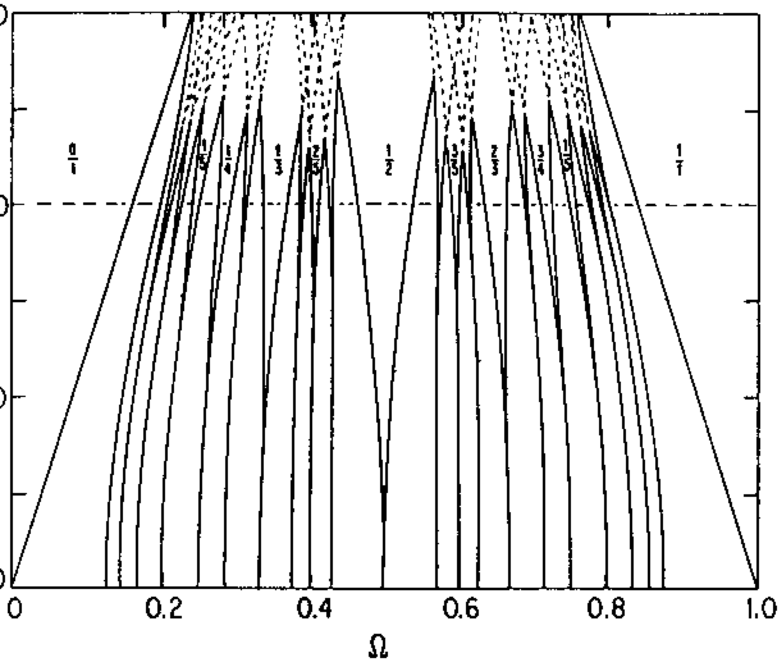

Figure 17. Mode-locked regions of the sine circle map. The corresponding ratios p/q are indicated. From Ref. 21.

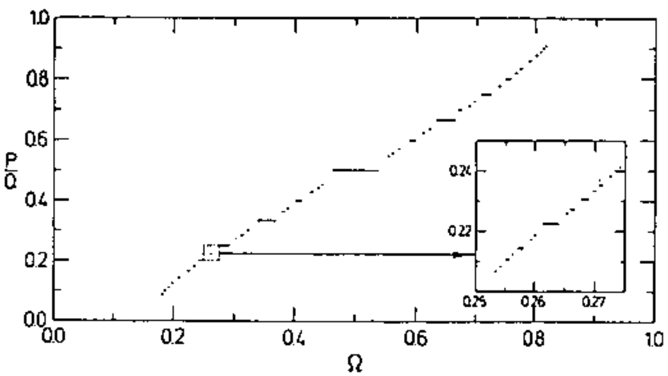

Figure 18. Devil's staircase. The structure is self-similar. From Ref. 20.

indicated by steps in the I-V curve. Analog computer solutions [26] of the Josephson equation, Eq. (3.3), have revealed that at $K = 1$, a mode locked interval with fractal dimension $d_F = 0.87$ is obtained, as suggested by the circle map. Chaos (as evidenced by hysteresis and noise in the I-V characteristics) has also been demonstrated in real junctions. [27]

In the case of charge density waves, the situation is quite complicated. For combined ac and dc electric drive fields, mode-locking is indeed observed, as illustrated in Fig. 19.[28] The flat-top peaks reflect the CDW phase being locked such that the CDW drift velocity is dictated by $v_d = \lambda_{CDW}\omega_{ex}p/q$, i.e. $\omega_{in}/\omega_{ex} = p/q$ over a finite range of E_{dc}. λ_{CDW} is the CDW wavelength. From data similar

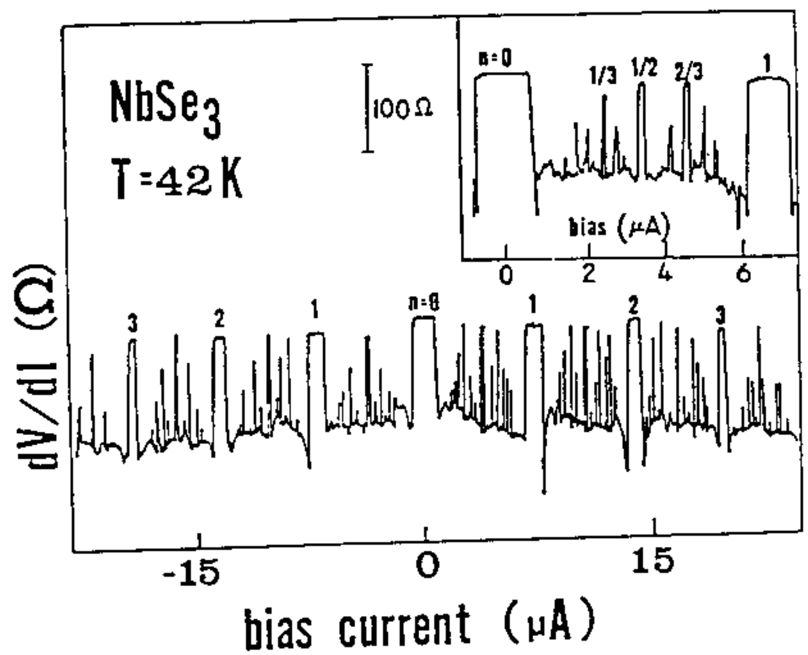

Figure 19. Mode locking in the CDW system $NbSe_3$. From Ref. 28.

that of Fig. 19, the fractal dimension of the complementary Cantor of the mode-locked region can be determined. This is performed as lows:[20-22] given a scale r, the total measure of the gaps between mode locked steps is $1 - S(r)$, and the number of "holes" is $N(r) = $ $- S(r)]/r$. If $rN(r) \longrightarrow 0$ as $r \longrightarrow 0$, the staircase is complete, with ctal dimension given by

$$N(r) \sim r^{-d_F} . \qquad (4.2)$$

arly analysis of $NbSe_3$ data by Brown et al.[29] yielded $d_F = 0.91$. recent studies [30] find that d_F depends strongly on ac drive itude, and actually approaches 1 as E_{ac} is increased. Chaos is not rved. This behavior is not entirely consistent with the circle and suggests that internal CDW degrees of freedom play an rtant role in the mode locking phenomenon.[31]

Figure 20a shows mode-locked regions (including harmonic and armonic structure) computed from coupled overdamped llators.[32] It is important to note that Eq. (3.5) does not ict subharmonic structure (nonintegral p/q ratio) in the damped limit. The behavior of Fig. 20a appears to be in good ement with that observed in real CDW systems. Hence, the CDW may more appropriately described as a set of coupled nonlinear llators, rather than a single anharmonic oscillator. As shown in 20b, even the set of coupled overdamped oscillators does not lay any positive Lyapunov exponents, and thus no chaos.

The CDW systems discussed so far are overdamped and do not in selves display chaotic response. The situation is very different CDW systems in the "switching" regime. In switching CDW's, phase centers are present in the crystal which dramatically alter the inear dynamics.[33]

Figure 21a shows mode-locked steps for $NbSe_3$ in the switching me. On each mode-locked step, a period doubling route to chaos is

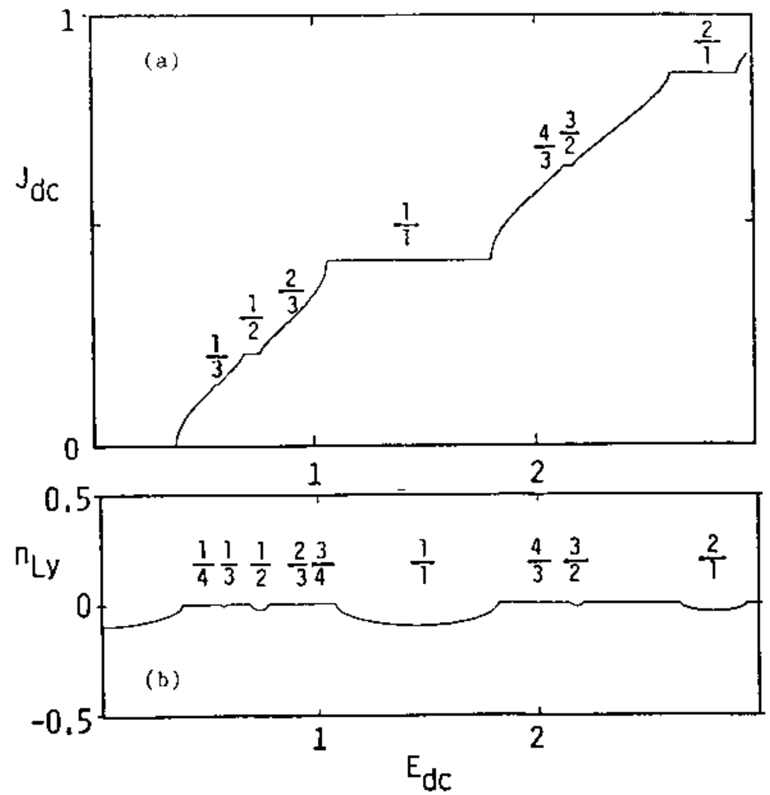

Figure 20. Locking in a system of two coupled oscillators. a) steps in I-V characteristics; b) Lyapunov exponents in mode-locked regions. No chaos is observed. From Ref. 32.

observed, as evidenced by the corresponding power spectra displayed in Fig. 21b. An interesting feature of the period doubling route is that it is observed to fully repeat on each new step; this behavior is consistent with the predictions of the circle map. In switching samples at large ac drive the fractal dimension of the mode locked steps approaches $d_F = 0.85$.[30] The routes to chaos in CDW systems, in

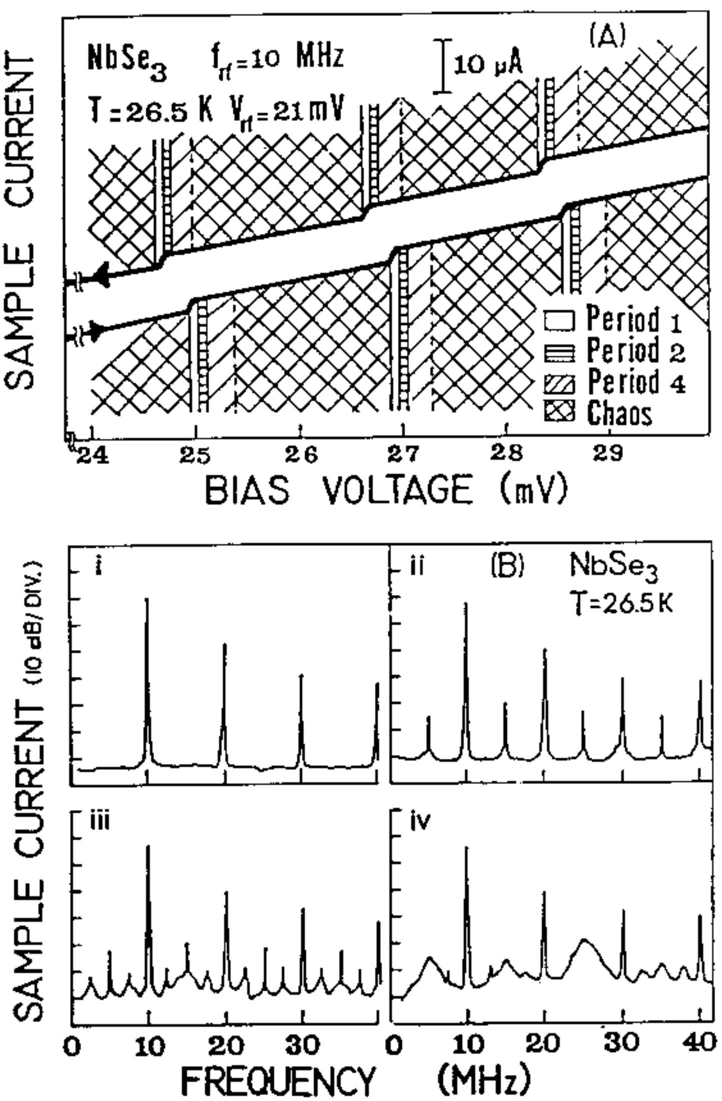

Figure 21. Period doubling route to chaos in $NbSe_3$. From Ref. 30.

particular dynamics in the switching regime, are largely unexplored, and should provide a bountiful area for future chaos research.

5. SEMICONDUCTORS

A great deal of very careful and beautiful work on nonlinear dynamics has recently been performed on semiconductor devices, including p-n junctions, photoconductors, and electron hole plasmas. The great precision with which the data can be collected allows detailed analysis, and hence these experiments have provided stringent tests of nonlinear dynamics theory.

Let us examine some "universal" predictions of nonlinear dynamics theory. The treatment is restricted to the period doubling route to chaos for a 1-D map with a single quadratic maximum. As a control parameter λ is increased, successive bifurcations occur, and eventually chaos is achieved. This is illustrated schematically in Fig. 22.

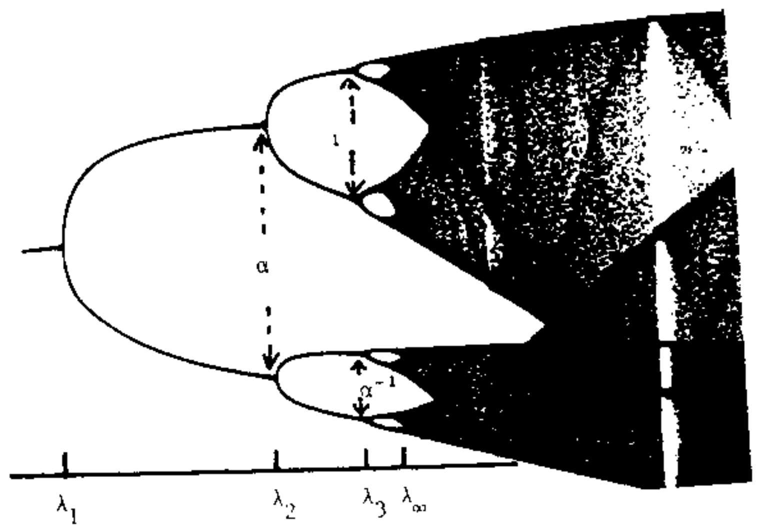

Figure 22. Bifurcation diagram.

eigenbaum [34] has predicted that there exists a well-defined scaling f the control parameter evaluated at the bifurcation points. At the irst bifurcation, $\lambda = \lambda_1$, at the second $\lambda = \lambda_2$, and so on. At $\lambda = {}_\infty$, the system goes aperiodic. It is suggested [34] that λ_n converges o λ_∞ geometrically, i.e.,

$$(\lambda_\infty - \lambda_n) \sim \delta^{-n} , \tag{5.1}$$

alid for large n, or that $\delta_n = (\lambda_{n+1} - \lambda_n)/(\lambda_{n+2} - \lambda_{n+1})$ converges to $\simeq 4.669$ as n becomes large. This value for δ is a "universal" umber, in that it should not depend on the details of the system.

A second universal number relates the vertical separation d of the furcation points on a bifurcation diagram, as illustrated also in g. 22. For large n, scaling exists [34] such that

$$\frac{d_{n+1}}{d_{n+2(+)}} = \alpha \ ; \ \frac{d_{n+1}}{d_{n+2(-)}} = \alpha^2 , \tag{5.2}$$

th $\alpha \simeq 2.502$.

A third universal number relates that heights (power) of new equency peaks which emerge during the period doubling sequence. As ccessive subharmonic frequency peaks are generated, their average ight is 10 log (20.963) = 13.21 db down from the height of the peak rresponding to the previous point.[35] The number 13.21 db presents a universal power loss.

We shall consider two more universal behaviors in the period ubling sequence. One is the amount of external noise power needed to duce by one the number of observable bifurcations; this turns out to a noise increase factor of N =6.55.[36] The second relates to noise ee "windows" in the bifurcation diagram as the control parameter is creased. For a 1-D map with a single extremum (not necessarily a

quadratic), a universal "U" sequence is followed.[37] Chaotic regions along λ-space are interrupted by regions of periodic behavior with no noise. Counting periods less than or equal to 6, the U-sequence is 1,2,4,6,5,3,6,5,6,4,6,5,6,..., where the numbers correspond to the period of the successive noise free windows.

The above features have been confirmed in numerical studies of various mappings. In the following section we shall test these features in a specific solid state system, the p-n junction.

5.1 P-N Junction

A p-n junction (diode) is a highly nonlinear device. When coupled to an external series resistance and inductance, the system can be driven into a chaotic state via a period doubling route.[38] Figure 23 shows a bifurcation diagram for a particular diode model. If the control parameter value at the bifurcation points is scaled according

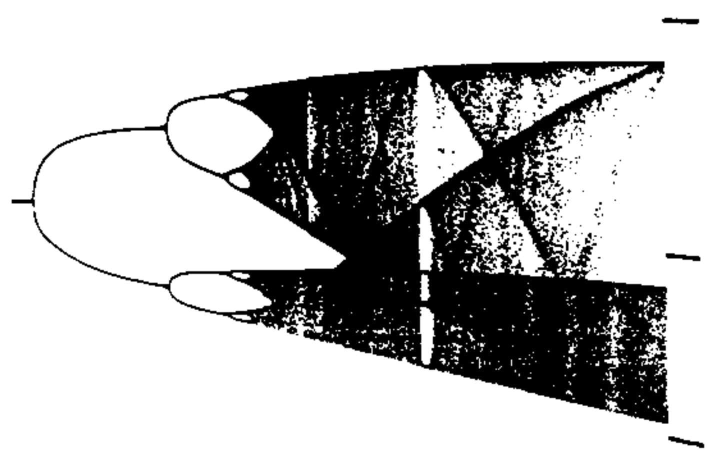

Figure 23. Bifurcation diagram for diode #300A. From Ref. 38.

Eq. (5.1), δ may be obtained. Similarly, α, N, and the power down
tio of the new frequency peaks can easily be determined. Table 5.1
mmarizes some of the experimental and theoretical results for these
rameters.[38] The experimental results are in surprisingly good
reement with theory (considering, for example, the limited range of n
ailable experimentally). The periodicity of noise free windows in
e bifurcation diagram has also been determined for various diodes.
observed sequence is 6,5,7,3,6,12,9,13, which is in exact agreement
th the U-sequence, starting at the first 6 (see above).

Number	Measured	Predicted
δ_1 } Eq. (3)	4.26 ± 0.1	4.751
δ_2	4.28 ± 0.1	4.656
δ_1 } Period 3	0.69 ± 0.1	0.979
δ_2 window	3.38 ± 0.1	4.429
α	2.41 ± 0.1	2.502
N	6.3 ± 0.3	6.55
Average spectral power ratio	11 to 15 dB	13.61 dB

Table 5.1. Universal numbers, as measured from p-n junctions and predicted from theory. From Ref. 38.

2 Coupled Oscillators

If a number of identical p-n junctions are coupled together and
ven from a single source, the resulting system may exhibit an
eedingly complex response spectrum.[39] Of particular interest is
possibility of Hopf bifurcations, which correspond to the birth of
imit cycle. Figure 24 shows schematically a Hopf bifurcation as a
trol parameter λ is varied. At the bifurcation point a new
commensurate) periodicity is exhibited. In practice, this results
a new, seemingly unrelated, frequency peak appearing in the response
er spectrum.

Van Buskirk and Jeffries[39] have extensively studied the dynamics

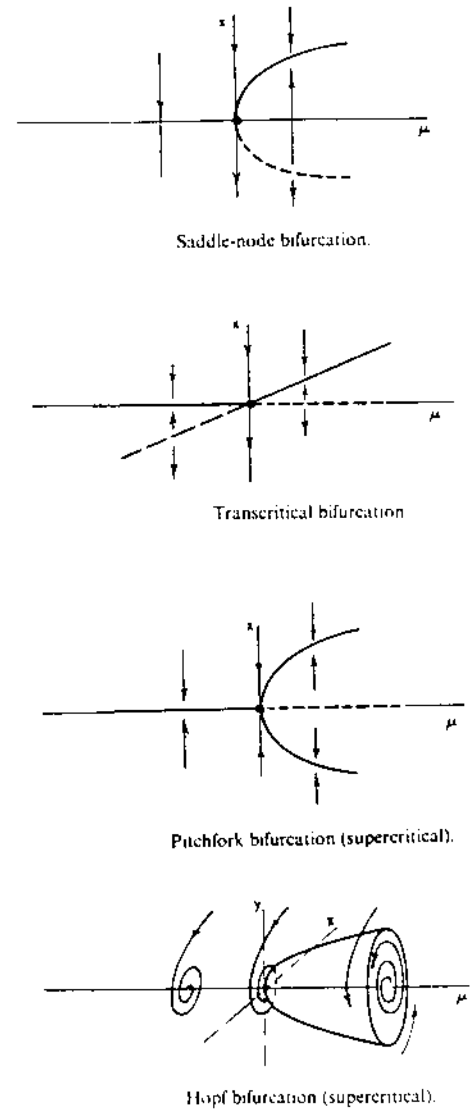

Figure 24. Co-dimension one bifurcations. The Hopf bifurcation corresponds to the birth of a limit cycle. Adapted from J. Guckenheimer and P. Holmes, Nonlinear Oscillations, Dynamical Systems, and Bifurcation of Vector Fields (Springer, New York, 1983).

f two coupled p-n junctions. For "resistively coupled" junctions, the ifurcation diagram displayed in Fig. 25 is obtained. For this system he initial period doubling is followed by a Hopf bifurcation (the dditional incommensurate frequency "fills up" the area between the iagram boundaries). This is followed by mode locking (or

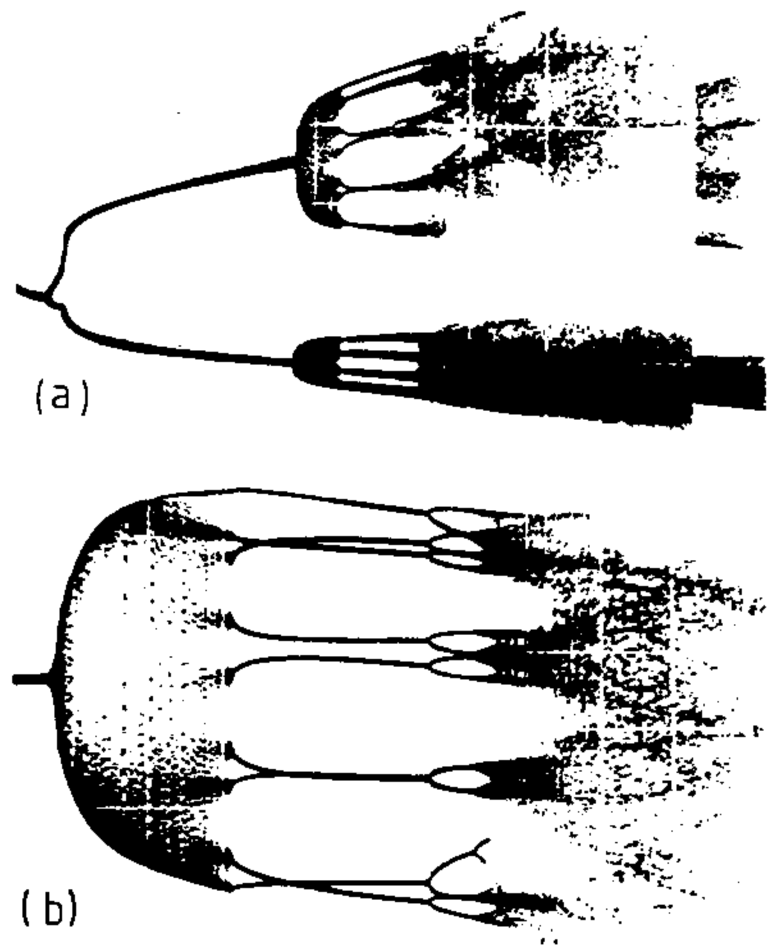

Figure 25. Bifurcation diagram for two coupled oscillators. From Ref. 39.

entrainment), two-band chaos, and finally crisis [40] of the attractor, i.e., a drastic change in the topological nature of the attractor. From the experimental data a "phase diagram" for the response of coupled p-n junctions can be constructed, as shown in Fig. 26. Note the complexity of this phase diagram when compared to the relatively simple circle map predictions of Fig. 17. A number of very beautiful data sets (phase

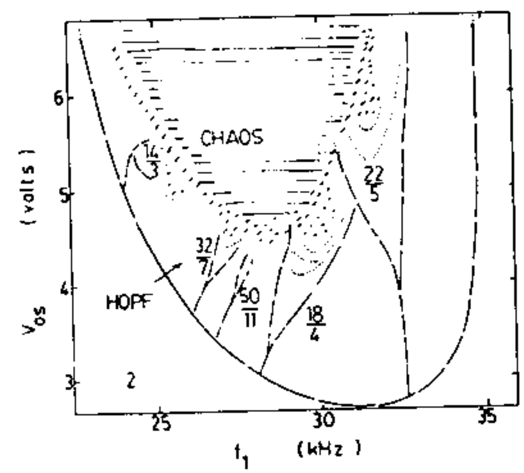

Figure 26. Phase diagram for coupled p-n junction oscillators. From Ref. 39.

portraits, Poincaré sections, bifurcation diagrams, etc.) have been obtained for coupled p-n junctions, and are described in detail in Reference 39. In this reference the p-n junctions are also modelled by various differential equations and return maps.

It should be noted that coupled p-n junctions bear a certain resemblance to some charge density wave compounds, where individual "oscillating" domains may be coupled together by normal electron resistive shunts. Phenomena such as Hopf bifurcations have yet to be explored in CDW systems.

.3 Photoconductors

Helium-cooled extrinsic photoconductors are often used as high-ensitivity, low-noise detectors of far infrared radiation. For this pplication, chaotic behavior is highly undesirable, but it does exist. rom a nonlinear dynamics point of view, photoconductors are thus of nterest. Chaos in photoconductors was first identified by Teitsworth t al.,[41] who found a period doubling route to chaos induced by an pplied dc field. Similar routes to chaos have also been obtained for c drive.

Figure 27 shows a phase portrait and corresponding power spectrum or an ac-driven Ge photoconductor, at various values of ac drive mplitude.[42] Both the phase plot and power spectrum indicate uccessive period doubling with increasing ac drive. In Fig. 28, the egions of different response are mapped out in the phase space of rive amplitude and drive frequency. The results of Fig. 27 and 28 are ell described by a simple and standard rate equation model for the hotoconductor,[43]

$$\dot{p} = \gamma(a - a_*) + pK(a - a_*) - pra_* , \tag{5.3a}$$

$$\epsilon E = J_{ext} - epv , \tag{5.3b}$$

$$p = a_* - d , \tag{5.3c}$$

$$J_{ext}(t) = J_0 + \Delta J \sin(\omega_{ex} t), \tag{5.3d}$$

here p is the hole concentration in the photoconductor, a is the total cceptor concentration, γ is the generation rate, K and r denote the

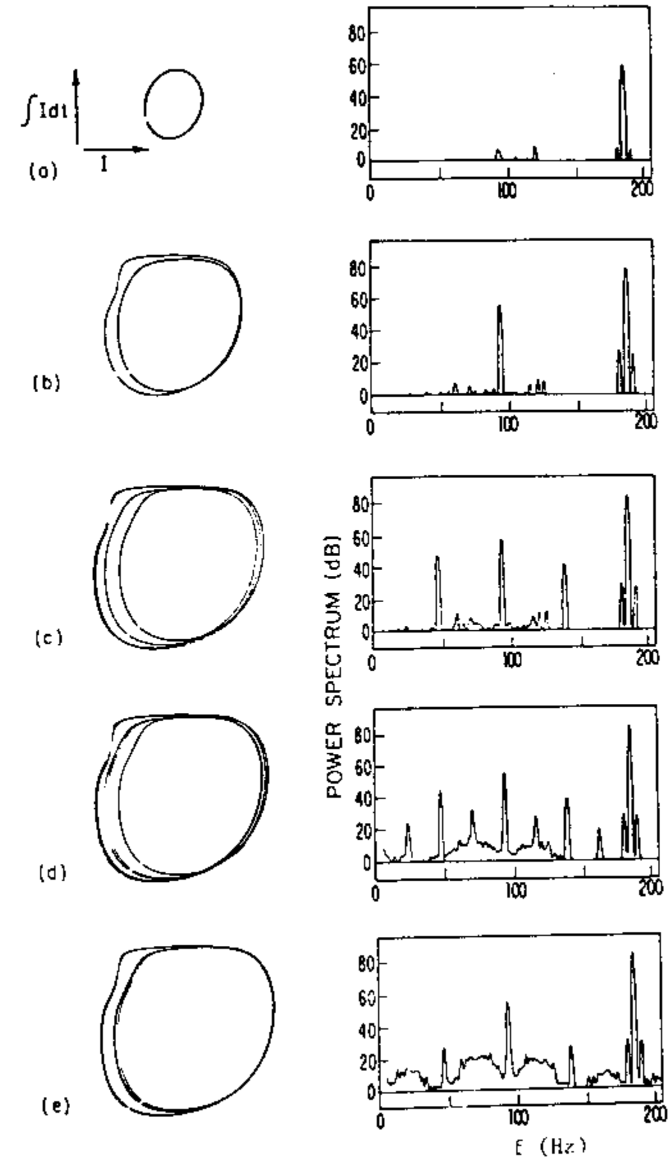

Figure 27. Response of Ge photoconductor for increasing ac drive amplitude. From Ref. 42.

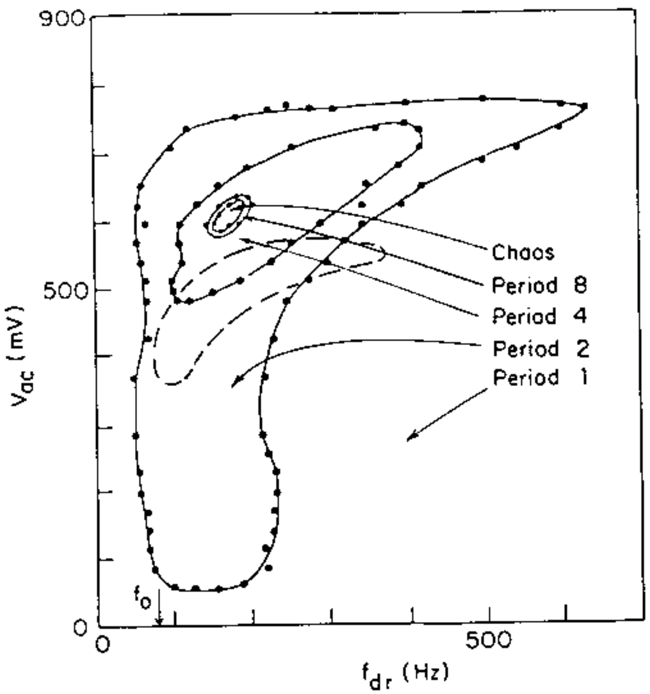

Figure 28. Response phase plot for Ge photoconductor. From Ref. 42.

field dependent impact ionization and capture rates, respectively, J_{ext} is the external current density, v is the carrier drift velocity, and ΔJ is the amplitude of the induced modulation current density. Numerical solution [43] of these equations produces the response displayed in Fig. 29. Figure 30 shows the corresponding Poincaré section and return map, and Fig. 31 shows the regions of periodic and chaotic response in the space of ac drive amplitude and drive frequency. Figure 31 may be qualitatively compared to the experimental data of Fig. 28. It is rather surprising that the set of simple standard equations (5.3) yield so complex a response, and in good qualitative agreement with experiment.

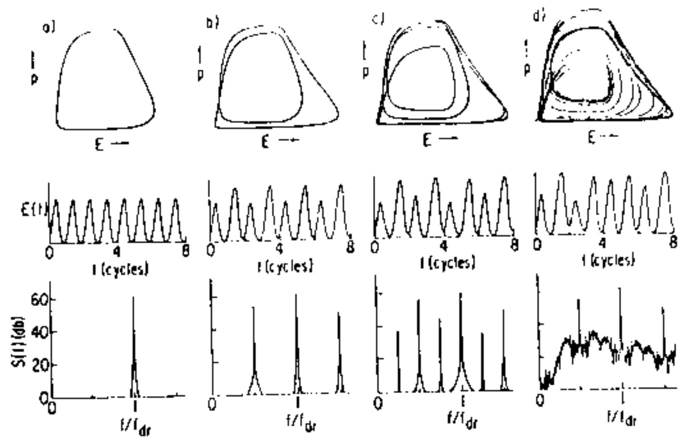

Figure 29. Phase portrait, real-time output, and power spectrum for photoconductor model, Eq. (5.3). From Ref. 43.

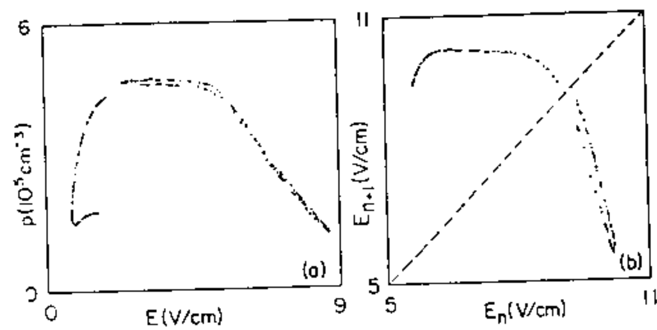

Figure 30. Poincaré section and return map generated from photoconductor model, Eq. (5.3). From Ref. 43.

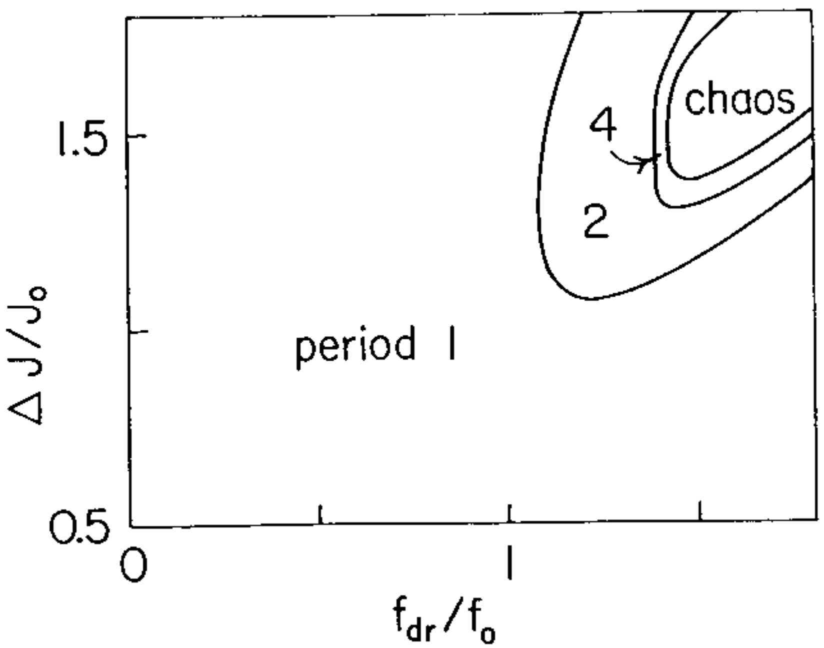

Figure 31. Response boundaries predicted by photoconductor model, Eq. (5.3). From Ref. 43.

.4 Electron-Hole Plasma

The electron-hole (e-h) plasma in Ge represents probably the first olid state system for which chaotic response has been studied patially as well as temporally. We consider first the e-h plasma in a ylindrical bar of semiconductor, with a long axis in the z direction, s illustrated in Fig. 32.[44] With applied parallel E_{dc} and H fields n the z direction, a screw-shaped helical wave is generated within the lasma, corresponding to a region of enhanced electron and hole lensity. The helical density is not stable, but may travel, thereby enerating internal oscillations within the specimen.[44]

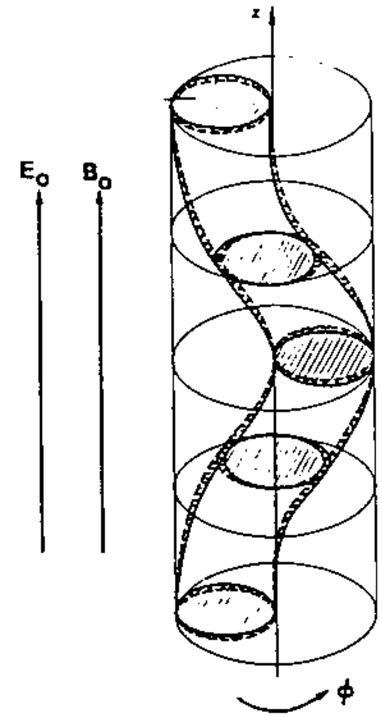

Figure 32. Helical plasma density in Ge. The electric and magnetic fields are along the axis of the specimen. From Ref. 44.

Various routes to chaos in the e-h plasma of Ge have been studied experimentally by Held and Jeffries,[45,46] using the geometry of Fig. 33. For the study of temporal chaos alone, the dc drive voltage V_{dc} is applied to the ends (injection contacts) of the bar. The system response is the current through the specimen. Both period doubling and quasi-periodic routes are observed.

Figure 34 shows an example of the period doubling route in the e-h plasma in Ge, with H = 4kG. The current response in real time, phase

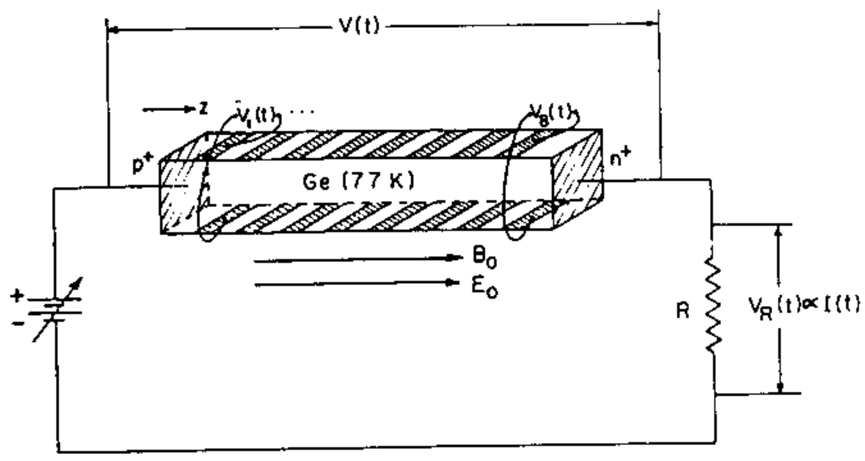

Figure 33. Experimental configuration for chaos measurements on electron hole plasma in Ge. From Ref. 46.

lots, and power spectra are shown. Fig. 34d corresponds to chaos, hile Fig. 34e corresponds to a period 3 window. The quasi-periodic oute to chaos is illustrated in Fig. 35. Here the experimentally etermined return maps $\{I_{n+1}, I_n\}$ and power spectra are shown. Onset f chaos is observed in Fig. 35d; "strong" chaos is apparent in Fig. 5f.

The fractal dimension of the attractor associated with chaotic ynamics in the e-h plasma has been computed experimentally, using the ethod outlined in Sec. 2.2. Some uncertainty arises because not all andomly chosen points from the reconstructed phase space yield the ame fractal dimension. Figure 36 shows a histogram of fractal dimension btained from 27 independent determinations of the fractal dimension or identical drive conditions.[46] The peak in the distribution uggests that the fractal dimension d_F lies between 2.4 and 2.6.

In Fig. 33, the Ge bar shown has a number of independent sensing robes along its length. These probes allow the investigation of patial chaos, i.e., the response can be spatially correlated. If the

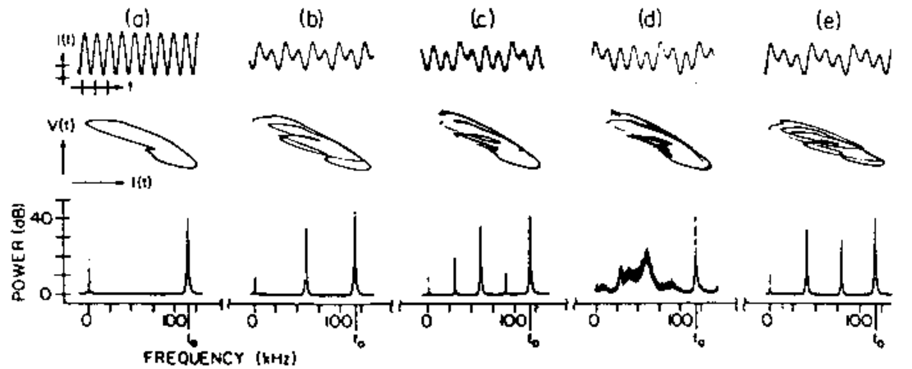

Figure 34. Period doubling route to chaos in e-h plasma in Ge. Real-time response, phase portraits, and power spectra are shown. The control parameter is the applied dc voltage. From Ref. 46.

temporal response were spatially coherent (regardless of the nature of the temporal response), then spatial correlation of the response would show only a phase shift, due to the coherent travelling e-h wave. The degree of spatial coherence is determined from a spatial correlation function[46]

$$C(r) = \left| \frac{2}{N} \sum_{n=1}^{N} V_i(n\tau)\, V_j(n\tau) \right|^{1/2} . \tag{5.4}$$

where $V_i(t)$ and $V_j(t)$ are the response voltages across two pairs of contacts separated by a distance r, t is the sampling interval, and N is a number large enough that C(r) has converged (typically, in these experiments, N = 20,000).

In the periodic regime of the driven e-h plasma, C(r) is that expected from a coherent travelling wave. However, in the (temporally) chaotic regime, there appears to be spatial breakup as well. Figure 37 shows C(r) versus V_{dc} for the e-h polasma for r = 4mm and 7mm.[46] At V_{dc} = 22V, C(r) has dropped well below that expected for spatiallly

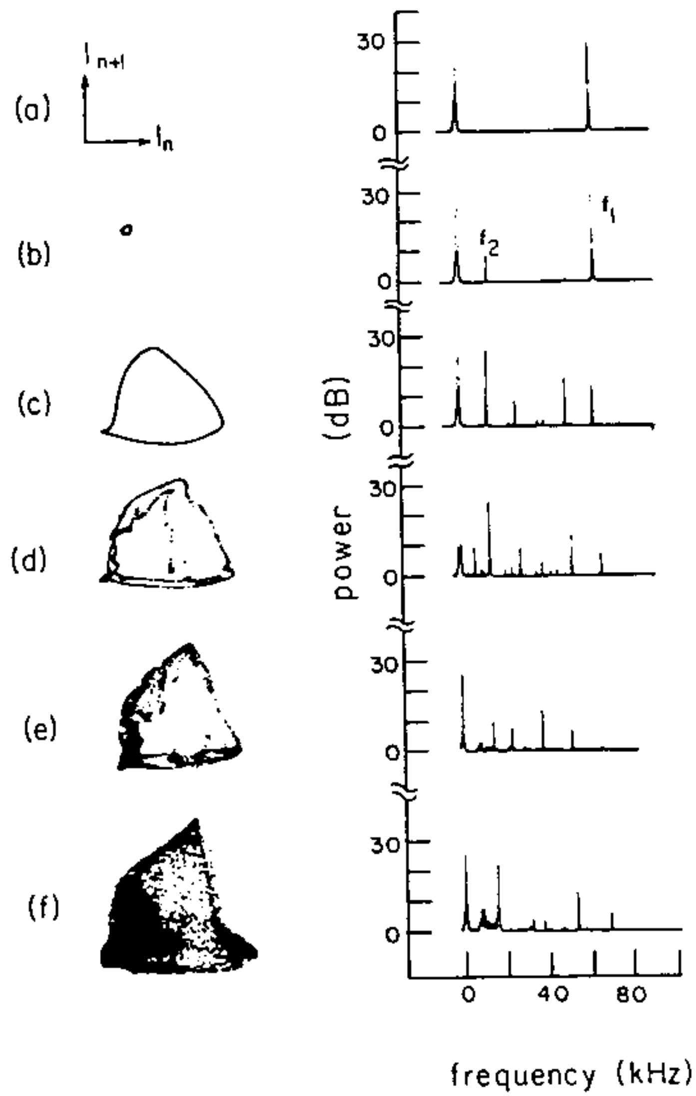

Figure 35. Experimentally determined return maps and power spectra for e-h plasma in Ge. A quasi-periodic route to chaos is indicated. From Ref. 46.

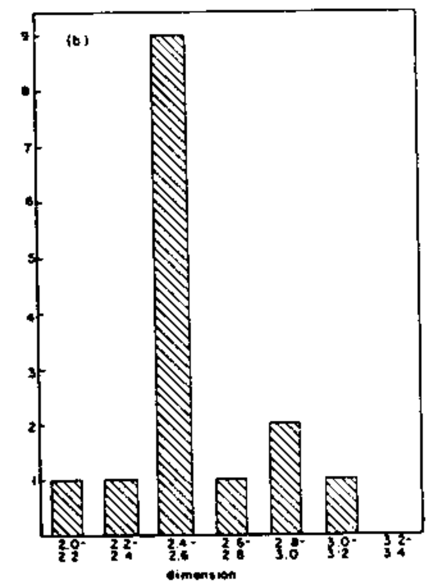

Figure 36. Dimension histogram for chaotic response in e-h plasma in Ge. From Ref. 46.

coherent response; this provides strong evidence for spatial chaos.

In the spatially chaotic regime of Ge, attempts have been made to determine the dimension of the attractor. Held [46] finds that just prior to breakup of the spatial coherence, the total current I(t) of the system is characterized by a low-dimensional attractor of dimension $d_F = 2.5$. Just after the onset of spatial disorder, dF is dramatically increased, with a lower limit of $d_F > 8$. The data for the determination of d_F in both cases is displayed in Fig. 38.

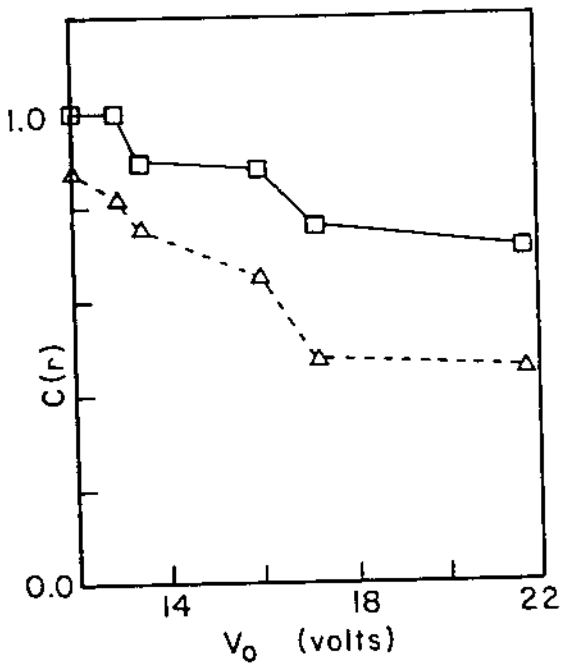

Figure 37. Spatial correlation versus dc drive in e-h plasma in Ge. From Ref. 46.

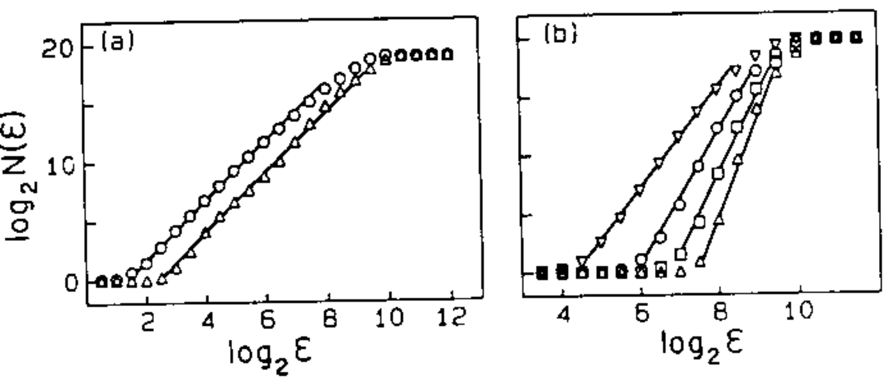

Figure 38. Fractal dimension determination for e-h plasma in Ge. a) in spatially coherent regime; b) in spatially turbulent regime. From Ref. 46.

The existence of spatial as well as temporal chaos no doubt exists in other solid state systems, such as magnetic chains and charge density waves. Indeed, recent experiments of the CDW system $NbSe_3$ have demonstrated that the source of the chaos (phase slip centers) corresponds to highly localized entities. [33)]

6. NOISE

One of the most notable features of chaos is of course the associated "noisy" response. In this section, we are interested not only in the noise generated by the chaos, but what influence <u>external</u> noise has on the system, in particular in the vicinity of a critical point. In Sec. 5, we have already encountered one external noise phenomenon: the amount of external noise needed to suppress the observation of one period doubling bifurcation. External noise (unrelated to noise generation by the chaos itself) can complicate noise analysis. For example, we have seen in the period doubling routes that a scaling relation exists for the parameter λ at bifurcation points. If noise is present, it may be difficult to determine exactly when the bifurcation takes place. One method of dealing with this problem is to asume that the period doubling peak amplitude in the Fourier transform scales as $(\lambda - \lambda_n)^{1/2}$, hence the peak height in the power spectrum scales as $\lambda - \lambda_n$. In practice one then needs only to measure the peak height over a small range of λ near λ_n, and extrapolate to zero height for λ_n.

In practice, the onset of a bifurcation (neglecting amplifier noise) is not always "clean", i.e. there often appears some sort of <u>noisy precursor</u> effect. In fact, the precursor effect can be <u>predicted</u> from chaos theory.

6.1 Noisy Precursor

Noisy precursor effects were first considered in detail by

Wiesenfeld.[47] We consider the effect of external Gaussian white noise of a nonlinear dynamical system. The noise acts as a stochastic perturbation on the forcing term, i.e., the limit cycle is not perturbed, and the phase space portaraits are "frozen in". Note that this approach is distinctly different from letting the parameters of the system fluctuate, which would lead to a fluctuation of the phase space portraits.

We here restrict ourselves to bifurcations of periodic orbits. In general we may write the perturbations in terms of eigenvectors

$$\phi^K(t) = e^{\rho_K t}\chi^K(t) \ , \tag{6.1}$$

where the exponential term is the <u>Floquet multiplier</u> and the χ term is periodic. If the limit cycle is stable, then we must have $Re(\rho_K) < 0$, i.e., the exponential term decays in time. There exist four kinds of bifurcations of periodic orbits: 1) transcritical ($Im\rho_K = 0$); 2) symmetry breaking ($Im\rho_K = 0$); 3) Hopf ($\rho_K = e + ib$); and 4) period doubling ($Im\rho_K = 1/2$). We shall consider the period doubling and Hopf cases.

Figure 39 shows a stable period T orbit x_o in phase space, along with the Poincaré section (single point). If the control parameter λ were increased, this orbit might undergo a period doubling bifurcation at λ_1. However, let us keep λ near to, but less than λ_1. If we now perturb the system, it will relax back. Successive intersections with the Poincaré plane will yield the Poincaré section displayed in Fig. 40. The points alternate back and forth about the limiting point. These transients have the character of a damped, <u>period 2T</u> orbit; hence the associated noise spectrum will show a broad bump at one half the fundamental frequency of x_o. Figure 41 shows the expected behavior for the power spectrum near a period doubling bifurcation. The "bump" structure just before the actual bifurcation is the noisy precursor.[47]

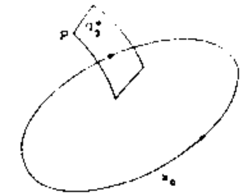

Figure 39. Stable period-one orbit. From Ref. 48.

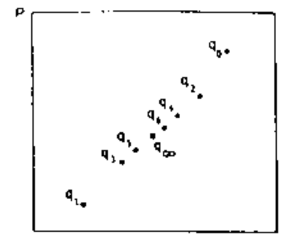

Figure 40. Successive intersections with Poincaré plane. From Ref. 48.

Another type of noisy precursor effect is the <u>virtual Hopf phenomenon</u>.[48] In this case, bump structure appears at two new frequencies, at $f_o - f'$ and f'. As the control parameter is varied, f' increases, until the two bumps coalesce into a bump at $f_o/2$, much like the bump of a period doubling precursor. This is followed by a period doubling bifurcation.

Noisy precursor effects have been observed experimentally in solid state systems. For example, Fig. 42 shows the noisy precursor effect in a p-n junction system, near a period doubling bifurcation.[49] Figure 43 shows the virtual Hopf phenomenon for the CDW system $NbSe_3$.[50] The control parameter here is the dc bias voltage.

6.2 Mode Locking and Chaos

In Figs. 12 and 21 it was demonstrated that chaos can exist on mode locked steps. An intriging question is whether or not the mode locked region is more or less likely to be sensitive to <u>external</u> noise. From the very terminology of a "locked" state, one might assume a resistance to external noise influence in the mode locked region.

We first examine the experimental situation for a mode locked CDW system. Figure 44a shows the differential resistance dV/dI and associated broad band noise for a dc driven CDW.[51] When the CDW

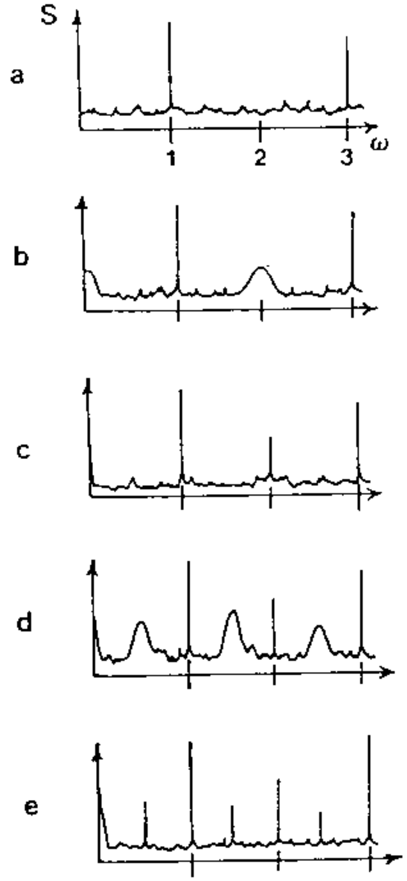

Figure 41. Noisy precursor associated with period doubling bifurcation. From Ref. 47.

moves, the noise voltage increases. Without discussing any microscopic reasons for such noise generation in CDW systems, we ask what happens to the noise amplitude when the CDW velocity is mode-locked. As shown

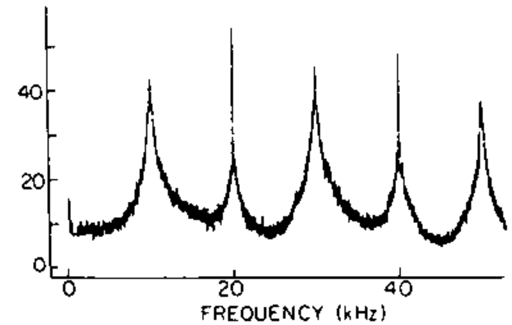

Figure 42. Noisy precursor in p-n junction. From Ref. 49.

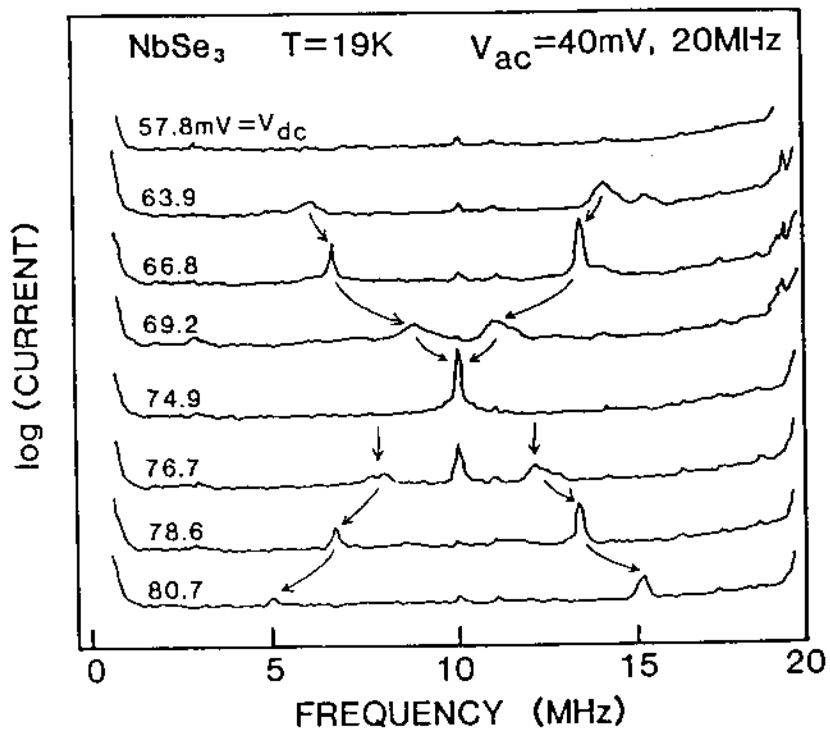

Figure 43. Possible virtual Hopf phenomenon in the CDW system $NbSe_3$. From Ref. 50.

in Fig. 44b, during mode-lock the noise vanishes identically! In a sense, the locking has frozen out the degrees of freedom generating the conduction noise.

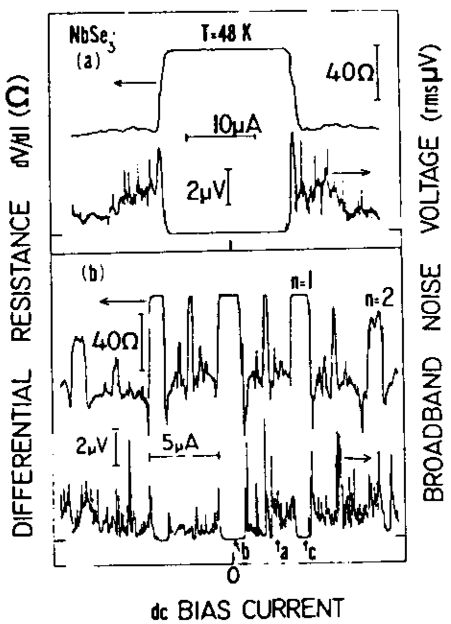

Figure 44. Mode locking and broad band noise in $NbSe_3$. a) no external ac drive; b) with external ac drive.

Wiesenfeld and Satija [52] have suggested that these observations in the CDW system represent a generic dynamical problem in nonlinear mode locking. As a simple example they consider a Poincaré section on the invariant circle (circle map). Figure 45a shows a 3 to 1 locking; Fig. 45b shows an unlocked case. Consider dynamics <u>along</u> the circle. The locked case may viewed as dissipative along the circle, while the unlocked case is non dissipative along the circle. If the locked system is perturbed, the system is damped and relaxes back to the 3

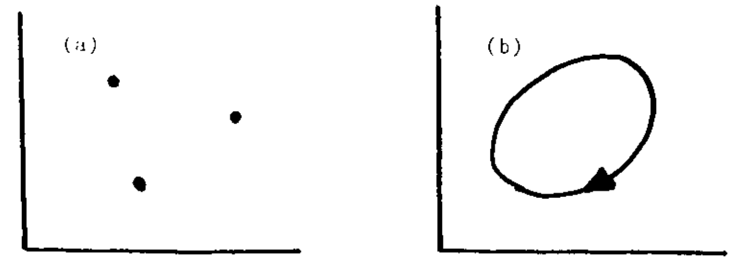

Figure 45. Circle map. a) 3 to 1 locking, fixed points shown. b) no locking. Adapted from Ref. 52.

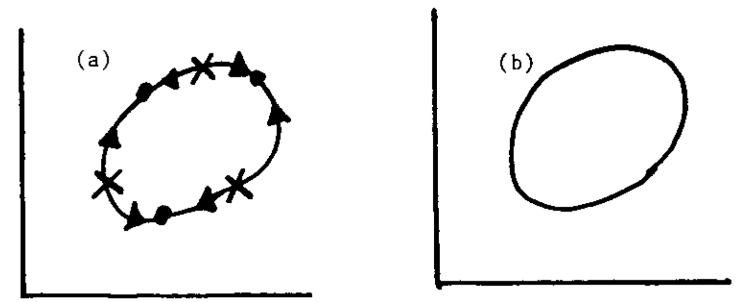

Figure 46. Dynamics along the circle map. a) locked regime: the perturbed system relaxes away from unstable fixed points to stable fixed points. b) no fixed points; system undergoes random walk about circle. Adapted from Ref. 52.

stable (and observable) fixed points (note that there exist also 3 unstable and unobservable fixed points; the system relaxes away from these). For the unlocked case, the 6 fixed points collide and annihilate in stable-unstable pairs. There is no relaxation of the perturbation, because no fixed points remain. This behavior is illustrated in Figs. 45a and 45b. In the unlocked case the noise produces a random walk away from the noise free orbit, and the perturbations accumulate with time. In contrast, in the locked case the noise produces perturbations which are damped out, leading to less sensitivity to external noise.

The CDW observations appear consistent with such an
terpretation. In fact, the CDW system may be an ideally suited
stem in which to test more precise predictions of the theory of
isenfeld and Satija, such as the response power spectra, etc. Mode
cking and noise in general should provide a very interesting line of
ture chaos research.

KNOWLEDGEMENTS

It is a pleasure to acknowledge stimulating discussions and
teractions with M.S. Sherwin, P. Bak, C. Jeffries, and M. Jensen
ring the course of this work. This research was supported by NSF
rant DMR 84-00041, and the Alfred P. Sloan Foundation.

EFERENCES

] Eckman, J.P., Rev. Mod. Phys. 53, 643 (1981).

] Ott, E., Rev. Mod. Phys. 53, 655 (1981).

] Farmer, J.D., Ott, E., and Yorke, J.A., Physica 7D, 153.

] Swinney, H.L., Physica 7D, 3 (1983).

] Packard, H.H., Crutchfield, J.P., Farmer, J.D., and Shaw, R.S., Phys. Rev. Lett. 45, 712 (1980).

] Grassberger, P., and Procaccia, I., Phys. Rev. Lett. 50, 346 (1983).

7] Huberman, B.A., and Crutchfield, J.P., Phys. Rev. Lett. 43, 1743 (1979).

3] For a review, see A. Barone and G. Paterno, Physics and Applications of the Josephson Effect, (Wiley - Interscience, New York, (1982).

9] Kautz, R.L., J. Appl. Phys. 52, 3528 and 6241 (1981).

[10] D'Humières, D., Beasley, M.R., Huberman, B.A., and Libchaber, A., Phys. Rev. A26, 3483 (1982).

[11] MacDonald, A.H., and Plischke, M., Phys. Rev. B27, 201 (1983)

[12] Octavio, M., Phys. Rev. B29, 1231 (1984).

[13] Goldhirsch, I., Imry, Y., Wasserman, G., and Ben-Jacob, E., Phys. Rev. B29, 1218 (1984).

[14] Huberman, B.A., Crutchfield, J.P., and Packard, N.H., Appl. Phys. Lett. 37, 750 (1980).

[15] Octavio, M., and Nasser, C.R., Phys. Rev.R30, 1586 (1984).

[16] For a review, see G. Gruner and A. Zettl, Phys. Rep. 119, 117 (1985).

[17] Gruner, G., Zawadowski, and Chaikin, P.M., Phys. Rev. Lett. 46, 511 (1981).

[18] Sherwin, M., Hall, R., and Zettl, A., Phys. Rev. Lett. 53, 1387 (1984).

[19] Shenker, S.J., Physica 5D, 405 (1982).

[20] Jensen, M.H., Bak, P., and Bohr, T., Phys. Rev. Lett. 50, 1637 (1983).

[21] Jensen, M.H., Bak, P., and Bohr, T., Phys. Rev. A30, 1960 (1984).

[22] Bohr, T., Bak, P., and Jensen, M.H., Phys. Rev. A 30, 1970 (1984).

[23] See, for example, B.B. Mandelbrot, The Fractal Geometry of Nature, (Freeman, New York, 1983).

[24] Jensen, M., et al., Phys. Rev. Lett. 55, 2798 (1985).

[25] Gwinn, E., and Westervelt, R., Phys. Rev. Lett. 57, 1000 (1986).

[26] Alstrom, P., Levinsen, M.T., and Jensen, M.H. Phys. Lett. 103A, 171 (1984).

[27] Miracky, R.F., Clarke, J., and Koch, R., Phys. Rev. Lett. 50, 586 (1983).

[28] Hall, R.P., and Zettl, A., Phys. Rev. B30, 2279 (1984).

[29] Brown, S.E., Mozurkewich, G., and Grüner, G., Phys. Rev. Lett. 52, 2277 (1984).

[30] Zettl, A., Physica 23D, 155 (1986).

[31] Coppersmith, S., and Littlewood, P., Phys. Rev. Lett. 57, 1927 (1986).

[32] Matsukawa, H., and Takayama, H., Syn. 19, 7 (1987).

[33] Hall, R.P., Hundley, M.F., and Zettl, A., Phys. Rev. Lett. 56, 2399 (1986).

[34] Feigenbaum, M.J., J. Stat. Phys. 19, 25 (1975); M.J. Feigenbaum, Physica 7D, 16 (1983).

[35] Nauenberg, M., and Rudnick, J., Phys. Rev. B24, 493 (1981).

[36] Crutchfield, J., Nauenberg, M., and Rudnick, J., Phys. Rev. Lett. 46, 933 (1981).

[37] Metropolis, N., Stein, M.L., and Stein, P.R., J. Comb. Theory Ser. A15, 25 (1973); see also Ref. 4.

[38] Testa, J., Pérez, J., and Jeffries, C., Phys. Rev. Lett. 48, 714 (1982).

[39] Buskirk, R., and Jeffries, C., Phys. Rev. A31, 3332 (1985).

[40] Grebogi, C., Ott, E., and Yorke, J.A., Phys. Rev. Lett. 48, 1507 (1982).

[41] Teitsworth, S.W., Westervelt, R.M., and Haller, E.E., Phys. Rev. Lett. 51, 825 (1983).

[42] Teitsworth, S.W., and Westervelt, R.M., Physica 23d, 187 (1986)

[43] Teitsworth, S.W., Westervelt, R.M., Phys. Rev. Lett. 53, 2587 (1984).

[44] Hoh, F.C., Lehnert, B., Phys. Rev. Lett. 7, 75 (1961).

[45] Held, G.A., Jeffries, C., and Haller, E.E., Phys. Rev. Lett. 52, 1037 (1984).

[46] Held, G., University of California Ph.D. Thesis (1985).

[47] Wiesenfeld, K., J. Stat. Phys. 38, 1071 (1985).

[48] Wiesenfeld, K., Phys. Rev. A32, 1744 (1985).

[49] Jeffries, C., and Wiesenfeld, K., Phys. Rev. A31, 1077 (1985).

[50] Zettl, A., Sherwin, M.S., and Hall, R.P., Physica 143B, 69 (1986).

[51] Sherwin, M.S., and Zettl, A., Phys. Rev. B32, 5536 (1985).

[52] Wiesenfeld, K., and Satija, I., Phys. Rev. B36, 2483 (1987).

NONLINEAR DYNAMICS AND CHAOS IN OPTICAL SYSTEMS

N.B. Abraham

Department of Physics

Bryn Mawr College

Bryn Mawr, PA 19010, U.S.A.

Two paradigmatic optical systems are considered as instructive examples from which we can learn about nonlinear dyanamics and chaos. In the first example, we will study a classic example of a nonlinear optical device with feedback which results in multiple steady state solutions for the same operating conditions. This system is the most frequently presented as an example for which the dynamics is well understood. Period doublings and chaotic behavior have been observed as predicted, but some subtle differences between experimental results and the theoretical predictions have forced revisions in the simple models that were initially put forward to explain the behavior. The second example is the case of a laser operating on a single mode. Here again the predictions are relatively simple and straightforward and we learn how the nonlinear field-atom interaction can lead to periodic and aperiodic modulation of the output. Although many lasers show periodic and chaotic modulation, experimental realizations of this model have been difficult to achieve. There is increasing evidence that there soon may be excellent working systems to compare with the predictions of the models.

CONTENTS